

1 **Oxygen Minimum Zones in the tropical Pacific across** 2 **CMIP5 models: Mean state differences and climate change** 3 **trends**

4
5 A. Cabré¹, I. Marinov¹, R. Bernardello^{1,2}, D. Bianchi^{3,4}

6 1. University of Pennsylvania, Philadelphia, USA

7 2. National Oceanographic Center, Southampton, UK

8 3. School of Oceanography, University of Washington, Seattle, USA

9 4. Department of Atmospheric and Oceanic Sciences, University of California Los Angeles,
10 Los angeles, USA

11

12 Correspondence to: A. Cabré (cabre@sas.upenn.edu)

13

14 **Abstract**

15 We analyze simulations of the Pacific Ocean oxygen minimum zones (OMZs) from 11 Earth
16 System model contributions to the Coupled Model Intercomparison Project Phase 5, focusing
17 on the mean state and climate change projections. The simulations tend to overestimate the
18 volume of the OMZs, especially in the tropics and Southern Hemisphere. Compared to
19 observations, five models introduce incorrect meridional asymmetries in the distribution of
20 oxygen including larger southern OMZ and weaker northern OMZ, due to interhemispheric
21 biases in intermediate water mass ventilation. Seven models show too deep an extent of the
22 tropical hypoxia compared to observations, stemming from a deficient equatorial ventilation
23 in the upper ocean combined with a too large biologically-driven downward flux of particulate
24 organic carbon at depth, caused by too high particle export from the euphotic layer and too
25 weak remineralization in the upper ocean.

26 At interannual timescales, the dynamics of oxygen in the eastern tropical Pacific OMZ is
27 dominated by biological consumption and linked to natural variability in the Walker
28 circulation. However, under the climate change scenario RCP8.5, all simulations yield small

1 and discrepant changes in oxygen concentration at mid depths in the tropical Pacific by the
2 end of the 21st century due to an almost perfect compensation between warming-related
3 decrease in oxygen saturation and decrease in biological oxygen utilization. Climate change
4 projections are at odds with recent observations that show decreasing oxygen levels at mid
5 depths in the tropical Pacific.

6 Out of the OMZs, all the CMIP5 models predict a decrease of oxygen over most of the
7 surface, deep and high latitudes ocean due to an overall slow-down of ventilation and
8 increased temperature.

9

10 **1 Introduction**

11 Most marine organisms suffer and might die in hypoxic conditions, i.e. when the oxygen
12 concentration falls below 60-80 mmol/m³ (Gray et al., 2002; Stramma et al., 2008). **Note that**
13 **this is a limited definition, since the specific survival and performance of organisms also**
14 **depends on the species, temperature, oxygen partial pressure, and CO₂ levels (Seibel, 2011).**
15 **However, a definition based on oxygen concentration facilitates the comparison across**
16 **models.** Oxygen minimum zones (OMZs) develop on the eastern outskirts of the subtropical
17 gyres owing to poor ventilation combined with high biological consumption, a consequence
18 of strong upwelling and biological productivity.

19 Two of the largest OMZs in the world are found to the north and the south of the equator,
20 respectively, in the eastern tropical Pacific. The northern (Costa Rica Dome) is the larger of
21 the two OMZs and is separated from the smaller one (west of Peru) by a well-ventilated
22 equatorial band (Karstensen et al., 2008; Paulmier and Ruiz-Pino, 2009; Fuenzalida et al.,
23 2009). The locations of the tropical Pacific OMZs are mostly determined by sluggish
24 ventilation, coinciding with a maximum in water age rather than a maximum in biological
25 productivity (Karstensen et al., 2008; Stramma et al., 2010b). As subtropical gyres prevent a
26 direct meridional ventilation of the OMZ, it is thought that eastward equatorial currents are
27 the most likely sources of oxygen to the OMZs (Stramma et al., 2010b). These equatorial
28 zonal jets are themselves fed by high latitude water masses. The northern tropical Pacific is
29 directly ventilated by the North Pacific Intermediate Water (NPIW), which, however, only
30 penetrates to a depth of 600 m, resulting in severe oxygen depletion below this depth. The
31 southern Pacific is mostly ventilated by water masses formed in the Southern Ocean, such as
32 the Antarctic Intermediate Water (AAIW) and the Subantarctic Mode Water (SAMW), which

1 ventilate mid-depth layers, and the Antarctic Bottom Water (AABW), which ventilates the
2 deep ocean.

3 A common problem in non eddy-resolving Earth System models is the merging of the
4 northern and southern OMZs in the tropics, resulting in large overestimation of the OMZ
5 volume relative to observations (Bopp et al., 2002; Matear and Hirst, 2003; Cocco et al.,
6 2013; Stramma et al., 2010a). This is related to the 'nutrient trapping' problem in coarse
7 resolution models (Najjar et al., 1992), where nutrients that accumulate in the subsurface due
8 to excessive remineralization feed the surface layers and promote new production. This
9 maintains high remineralization rates and, in the absence of a vigorous horizontal circulation,
10 anomalously high nutrient pools in the subsurface.

11 It is hard to distinguish to what extent the OMZ biases in models are driven by physical and
12 biogeochemical processes, or a combination of both. Najjar et al. (2007) found large
13 differences in oxygen, particulate organic carbon (POC), and dissolved organic carbon (DOC)
14 when comparing 12 different circulation models with the same biogeochemical module. On
15 the other hand, Kriest et al. (2010, 2012) studied the sensitivity of a fixed physical ocean
16 model to changes in biogeochemical parameters related to oxygen loss, also finding large
17 differences in the shape of OMZ. These studies reveal that both physical and biogeochemical
18 causes modify the oxygen concentration and the shape of the OMZ, making it difficult to
19 isolate the different contributions when comparing models with both different physics and
20 biogeochemistry, as in the current study.

21 With climate change, increased temperatures result in decreased O₂ solubility (thermal effect)
22 while an increase in stratification is expected to reduce the ventilation of the subsurface and
23 hence O₂ concentration (Keeling and Garcia, 2002). Significant global deoxygenation over the
24 past 50 years has been observed (Helm et al., 2011) together with expansion of the OMZ in
25 the North Pacific (Ono et al., 2001; Emerson et al., 2004; Whitney et al., 2007; Chan et al.,
26 2008; Pierce et al., 2012) and in the southern California Current System (Bograd et al., 2008;
27 McClatchie et al., 2010), with the largest relative O₂ declines occurring below the thermocline
28 in the tropical oceans (Stramma et al., 2008; Stramma et al., 2010b; Stramma et al., 2012).
29 While observations show a clear ongoing decline of oxygen in the tropical thermocline,
30 previous Earth System model studies show a small change or even an increase of oxygen
31 there with warming (Bopp et al., 2002; Matear and Hirst, 2003; Cocco et al., 2013; Bopp et
32 al., 2013) with a small associated change in OMZ volume. **The expansion of low-oxygen**

1 zones will result in the transition, adaptation, and/or extinction of different species in the real
2 ocean.

3 The wide range of physical and biogeochemical characteristics across CMIP5 models offers a
4 unique opportunity to understand common and persistent biases in state-of-the-art resolution
5 Earth System simulations. In this study, we analyze 11 Earth System Models participating in
6 the *Coupled Model Intercomparison Project Phase 5 (CMIP5)*, Taylor et al., 2012) to identify
7 the common mechanisms involved in the creation of OMZ biases in the eastern tropical
8 Pacific, as well as the response of the respective OMZs to interannual variability and climate
9 change. We compare models with observations, analyze potential sources of bias across
10 different models, and provide recommendations for improving OMZ representation. Methods
11 are described in Section 2. Results are summarized in Section 3 and include historical biases
12 in the description of Pacific OMZs across CMIP5 models (Section 3.1), 21st century
13 predictions (Section 3.2), and interannual variability (Section 3.3). The full, model-by-model
14 analysis of the physical and biological processes influencing the position and extension of
15 OMZs is presented in the Appendix. Based on literature review and our own analysis we
16 summarize in Tables A2 and A3 descriptions of (a) relevant ventilation sources and (b) bio-
17 chemical parameters and processes that affect OMZs across the CMIP5 models analyzed.

18

19 **2 Methods**

20 *Earth System Simulations*

21 We examine simulations from 11 non-eddy resolving CMIP5 Earth System Models,
22 downloaded from <http://pcmdi9.llnl.gov/esgf-web-fe/> (detailed in Table A1). In order to
23 estimate 100-year trends, our analysis compares simulations for the period 1960-1999
24 (hereafter called “present”) to simulations for the period 2060-2099 (hereafter called
25 “future”). We assume that the 40-year periods are sufficiently long to ensure that natural
26 variability is smoothed out. **The historical period is chosen around 1980 for a direct
27 comparison to observations.** The “present” output is taken from the “Historical” experiment
28 (years 1850 to 2005), while the “future” output is taken from the Representative
29 Concentration Pathway 8.5 experiment (hereafter called RCP8.5, years 2006 to 2100),
30 detailed in Meinshausen et al. (2011). Atmospheric CO₂ concentrations are based on observed
31 and reconstructed values for the Historical experiment while RCP8.5 values are based on CO₂

1 emissions resulting in a radiative forcing of 8.5 W/m^2 by the end of the 21st century (Riahi et
2 al., 2011).

3 Our selection of models was then limited to those that included the variable “o2” (“oxygen
4 concentration”) and output for both the Historical and RCP8.5 experiments, and had reached
5 equilibrium (no significant trends during the period 1850-1950). One of the analyzed models,
6 MRI-ESM1, did not provide RCP8.5, so the esmRCP8.5 scenario, which explicitly computes
7 CO₂ levels from anthropogenic emissions (Friedlingstein et al., 2014), was used instead in this
8 case. For Section 3.3, we created a control time series to study natural interannual variability
9 by de-trending the Historical run from 1900 to 1999 from its climate signal (calculated as the
10 20-year running mean).

11 *Observations*

12 We used oxygen (O₂), Apparent Oxygen Utilization (AOU), saturated oxygen (O₂sat), nitrate,
13 phosphate, salinity, and temperature climatologies from the World Ocean Atlas 2009 database
14 (https://www.nodc.noaa.gov/OC5/WOA09/pr_woa09.html). We applied a correction to
15 oxygen concentrations, which were found to be overestimated in gridded WOA data (Bianchi
16 et al., 2012). Sea level pressure was provided by the NOAA/OAR/ESRL PSD dataset at
17 <http://www.esrl.noaa.gov/psd/> (Kaplan et al., 2000). Water-mass age [yr] was calculated from
18 radiocarbon deficit (¹⁴C [‰]), downloaded from the Global Ocean Data Analysis Project
19 database (<http://cdiac.ornl.gov/oceans/glodap/>), as $\text{age} = -8033 \ln(1 + ^{14}\text{C}/1000)$. Since we
20 only use it as a qualitative reference, there is no need of further calibration. The climatology
21 of the equatorial component of the water current velocity (u [m/s]) was taken from Johnson et
22 al. (2002).

23 In order to compare models with observations, we calculated for each model simulation O₂sat
24 from the in-situ temperature and salinity (Garcia and Gordon, 1992); O₂sat represents the
25 oxygen concentration in equilibrium with the atmosphere at a given temperature and salinity.
26 The Apparent Oxygen Utilization (AOU) was then computed as the difference between O₂sat
27 and O₂ (AOU=O₂sat- O₂). AOU for a parcel of water represents the accumulated oxygen
28 consumption since the parcel left the surface along the ventilation pathway, assuming that O₂
29 was saturated at the time the parcel was last in contact with the atmosphere. We note that
30 AOU is not the real oxygen consumption given that most waters are undersaturated in zones
31 of deep-water formation (Ito et al. 2004), but provides a good approximation.

1 Particulate organic carbon export was obtained from satellite-derived estimates calibrated
2 with in situ export measurements from shallow traps (Dunne et al., 2005) and thorium-based
3 methods (Henson et al., 2012), and by combining satellite observations and food-web models
4 in Siegel et al. (2014).

5

6 For both models and observations, stratification was calculated as the difference in the
7 potential density [kg/m^3] of seawater between the depth of 200 m and the surface. The Walker
8 circulation index was defined as the difference between the sea level pressure at the eastern
9 tropical Pacific ($160^\circ\text{W} - 80^\circ\text{W}$ and $5^\circ\text{S} - 5^\circ\text{N}$) and the western tropical Pacific ($100^\circ\text{E} - 160^\circ\text{E}$
10 and $5^\circ\text{S} - 5^\circ\text{N}$) as in Vecchi et al. (2006).

11 *Agreement across models*

12 The multi-model mean is calculated as the average value across all the CMIP5 models in the
13 period 1960-1999, with a simple weight applied to avoid repeating models that are known to
14 be very similar (Table A1, Cabré et al., 2014).

15 To quantify agreement among the models in the predicted 100-year change, we use a
16 bootstrapping statistical technique. In our bootstrap sampling, each realization is the weighted
17 average over N models that are selected randomly with replacement among the N available
18 models. We represent inter-annual variability by randomly picking one of the 40 years in the
19 present (1960-1999) and future (2060-2099) each time that we randomly select a model. For
20 each studied variable at each point in the ocean, we create 1000 realizations of the resulting
21 100-year trend and obtain the multi-model significance of this trend using the percentage of
22 realizations that predict a trend above or below zero (details in Cabré et al., 2014).

23

24 **3 Results and Discussion**

25 **3.1 Comparison of observed and predicted OMZs in the CMIP5 models during** 26 **the historical period (1960-1999)**

27 The comparison between CMIP5 model oxygen simulations and WOA09 observations
28 highlights several consistent biases (Fig. 1 and Fig. 2). **(a)** A majority of the models join the
29 northern and southern OMZ regions into a single large tropical OMZ (Fig. 1a), such that the

1 modeled OMZ reaches anoxic conditions at shallower depths (Fig. 1c-d), and expands more
2 westward and deeper than observed (Fig. 1c-d). (b) In observations, the northern OMZ area
3 and volume are much larger than the southern counterpart, while in models the northern and
4 southern OMZ areas and volumes are much more symmetric with respect to the equator (Fig.
5 1a-b). A reason for this is a bias in the modeled Southern Hemisphere OMZ, systematically
6 larger than observed **except for the IPSL models** (Fig. 1a-c, Fig. 2). In addition, in some
7 models (namely, GFDL-ESM2G, GFDL-ESM2M, HadGEM2, NorESM1-ME, and MRI-
8 ESM1) the Northern Hemisphere OMZ is often too small in horizontal extent or does not
9 extend as deep as in observations (Fig. 2). (c) A subset of models (GFDL-ESM2G, GFDL-
10 ESM2M, MPI-ESM, and NorESM1-ME) produce anoxia to a depth of 2500 m or more in the
11 eastern tropical Pacific, which is deeper than observations by more than 1500 m (Fig. 1c-d
12 and Fig. 2).

13 Fig. 3 shows the modeled and observed vertical distributions of oxygen, phosphate, and
14 nitrate averaged over the eastern tropical Pacific (a, b, c) and the world ocean (d, e, f). Note
15 the large dispersion of the modeled values in the eastern tropical Pacific despite a good
16 agreement at the global scale. Models that simulate anomalously deep OMZs yield too low
17 oxygen levels at intermediate depths compared to observations and too much phosphate
18 trapped at depth. Concurrently, such low levels of oxygen in these models trigger
19 denitrification, reducing nitrate to anomalously low levels.

20 We discuss in the following the main potential causes for the aforementioned biases. The full,
21 model-by-model analysis of the physical and biological processes influencing the position and
22 extension of OMZs is presented in detail in Appendix 1 and Tables A1, A2 and A3 of the
23 Appendix 2.

24 **3.1.1 Physical causes for OMZ biases in historical simulations**

25 In this section we explore differences between models and observations in ventilation
26 patterns, mixing coefficients, and ocean-model resolution, all of these possible physical
27 causes for OMZ model biases.

28

29 *Underestimated Equatorial Undercurrent*

30 The complex system of equatorial currents is dominated by the Equatorial Undercurrent
31 (EUC), the strong subsurface eastward current shown in observations in the last panel of Fig.

1 4. On one hand, the EUC determines the depth of the tropical Pacific OMZ in the west-east
2 direction and controls most of the ventilation with O₂ to the tropical OMZ (Aumont et al.
3 1999). On the other hand, the EUC is responsible for bringing the nutrients that enhance
4 biological productivity and subsequent consumption of organic matter on the eastern side of
5 the basin, contributing to OMZ formation and opposing the ventilation effect. As an example,
6 the underestimate of subsurface OMZ volume in the IPSL-CM5A models (Fig. 1a-b) might be
7 related to the fact that nutrients (and hence primary production and POC flux) are
8 underestimated there **when compared to the rest of CMIP5 models** (Fig. 3b and Fig. 5)
9 probably due to a weak EUC (Fig. 4).

10 All CMIP5 models show that EUC weakens too much before reaching the eastern side of the
11 basin (Fig. 4), which contributes to weaker eastern ventilation compared to observations.
12 However, we find that the models having the most accurate representations of the EUC flow
13 (NorESM1-ME and MPI-ESM-MR) still produce too large OMZs, pointing to other causes
14 for OMZ bias. Despite the bias in EUC strength, the EUC is better modeled than the rest of
15 equatorial currents and not thought to be the main cause for the large OMZ across simulations
16 (Dietze and Loeptien 2013). A comparison between EUC flow and Pacific OMZ size at mid-
17 depths across CMIP5 models showed no correlation.

18 Increased resolution improves the representation of equatorial currents (especially the EUC;
19 Aumont et al., 1999), which is evident when comparing MPI-ESM-LR (coarse resolution
20 model) and MPI-ESM-MR (quasi-eddy resolving resolution, 0.4°) in Fig. 4 (see also
21 Jungclaus et al. 2013). However, both versions of MPI-ESM model show similar biases in
22 oxygen distribution and a too deep tropical OMZ (Fig. 1), **which suggests that the too-deep**
23 **modeled OMZ is not linked to the strength of equatorial currents but set by high-latitude**
24 **ventilation processes or/and biological biases at low latitudes**. Both IPSL-CM5A models, with
25 low ocean resolution of ~2°, show similarities with MPI-ESM-LR (same ~2° resolution) in the
26 characterization of a diffuse and weak EUC and nonexistent deep jets. The rest of models
27 have oceanic resolution of ~1°, higher than the IPSL-CM5A and MPI-ESM-LR models' one
28 (Table A1), and hence provide a more accurate **representation** of EUC compared to
29 observations.

30

31 *Deficient equatorial (non-EUC) ventilation*

32 **In general, the non-EUC equatorial jets are also too weak or in some cases nonexistent in non**

1 eddy-resolving models (compare CMIP5 models and observations in Fig. 4). This complex
2 equatorial system is formed by the eastward Northern and Southern Subsurface
3 Countercurrents (SCCs, also known as Tsuchiya jets in the Pacific; Tsuchiya, 1981) - shown
4 as shallow currents at 6°N-8°N and 6°S-8°S in the last panel of Fig. 4, the westward northern
5 and main branches of the South Equatorial Current (SEC(N) and SEC) - on both sides of the
6 EUC in Fig. 4 - , and deeper currents as described in detail for example in Stramma et al.
7 (2010b).

8 In observations, the north and south equatorial countercurrents (SCCs) determine the
9 separation between the well-ventilated tropics and the low-latitude OMZs (Fig. 1a). However,
10 because of the deficient equatorial circulation in the models (Fig. 4), most models tend to join
11 the northern and southern OMZ cells – well separated in observations – into a single large
12 tropical OMZ (Fig. 1a). We suggest that consequences of the too slow lateral ventilation of
13 these regions in CMIP5 models include too low subsurface oxygen concentration (Fig. 3a)
14 and too large nitrate depletion due to excessive denitrification kicking in when O₂ falls below
15 a certain threshold (Fig. 3c, compare black and colored lines). **The low ventilation exacerbates**
16 **nutrient trapping and potential for runaway feedbacks in the nitrogen cycle (Landolfi et al.**
17 **2013).** The CMIP5 models also underestimate the strength of westward subsurface equatorial
18 jets (SECs), which in the real ocean contribute to carrying nutrients away from the OMZ, thus
19 alleviating the large oxygen deficit and nutrient trapping in the tropical OMZ. Finally, CMIP5
20 models do not capture the fine structure of the deep equatorial jets thus underestimating lateral
21 advection and mixing along the equator and contributing to the expansion of OMZs.
22 Consequently, all models except for the IPSL-CM5A models show a sub-surface excess of
23 phosphate in the Pacific tropics (Fig. 3b). Dietze and Lopetien (2013) also speculate that
24 nutrient trapping is caused by a poor representation of the Equatorial current system in
25 models, with the exception of the EUC. Montes et al. (2014) show the crucial role of the
26 secondary Tsuchiya jets (sSSCC, subsurface current at ~9°S) in the ventilation of the OMZ off
27 Peru. A good balance between oxygen-poor transport by sSSCC and oxygen-rich transport by
28 EUC is crucial to describe the position and extent of this OMZ. Similarly, **Duteil et al. (2014)**
29 **highlight the need for accurate deep Equatorial ventilation, in addition to EUC, to characterize**
30 **the eastern tropical Atlantic OMZ.**

31 Some recent studies showed that the equatorial ventilation is not fully resolved even in eddy-
32 resolving models (Brandt et al., 2008; Eden and Dengler, 2008; Ascani et al., 2010),

1 suggesting that other mechanisms such as submesoscale dynamics, or atmosphere-ocean
2 feedbacks might also be responsible for biases in the equatorial jets and their incomplete
3 representation in models (Lin, 2007; Li and Xie, 2014; Ridder and England, 2014).

4 5 *Inadequate ventilation from the Southern Ocean and North Pacific*

6 The Pacific Ocean equatorial circulation is fed by intermediate water masses formed in the
7 Southern Ocean (AAIW, SAMW) and North Pacific (NPIW). In observations, the northern
8 tropical Pacific OMZ is larger and deeper than the one south of the equator, because the
9 former receives disproportionately less oxygen via the large-scale circulation pathways
10 (Karstensen et al., 2008).

11 Sallee et al. (2013b) reported large variations in Southern Ocean water masses formation
12 across CMIP5 models. We find also considerable inter-model variability in the zonally
13 averaged vertical distribution of oxygen (Fig. 2). Most CMIP5 models overestimate the size
14 of the southern tropical Pacific OMZ, which develops at shallower depths than observed (Fig.
15 1c), partly due to deficient intermediate water ventilation from the Southern Ocean, reinforced
16 by excessive biological export and remineralization. Previous studies have pointed out that, in
17 current coarse resolution models, the AAIW and SAMW do not extend sufficiently northward
18 in the Pacific (Salée et al., 2013b; Downes et al., 2010), in agreement with our findings.

19 Some models (namely, GFDL-ESM2G, GFDL-ESM2M, HadGEM2, NorESM1-ME, and
20 MRI-ESM1) overestimate oxygen levels north of the tropical OMZ in addition to
21 underestimating oxygen in the low-latitudes Southern Hemisphere (Fig. 2). The observed
22 deep anoxic zones in the Northern Hemisphere (at depths between 600 m and 1200 m) are not
23 found in these models due to excessively deep ventilation by AABW-fed flow from the
24 Southern Ocean to the deep North Pacific and/or an excessive mixing of NPIW with deep
25 waters (see details and references for individual models in Table A2). For example, models
26 with excessively deep AABW ventilation (such as NorESM1-ME and GFDL-ESM2G) or
27 excessive NPIW ventilation (such as GFDL-ESM2M) have a reduced extent of the North
28 Pacific OMZ. On the other hand, deficient NPIW ventilation, as in CESM1-BGC, exaggerates
29 the volume of OMZs in the Northern Hemisphere (Fig. 2 and Table A2).

30 However, the anomalously deep OMZ found in some models in the tropics (Fig. 1c-d and Fig.
31 2) does not seem related to ventilation sources such as AABW, AAIW, or NPIW, as models

1 having a similar biogeochemical module (MPI-ESM and NorESM1-ME) show similar OMZ
2 extent despite having significantly different representations of different water masses
3 (Appendix Table A2). For example, NorESM1-ME shows one of the highest deep O₂ levels
4 but still develops a deep OMZ (Fig. 2). This problem is discussed in Section 3.1.2.

5

6 *Inadequate representation of isopycnal mixing*

7 Gnanadesikan et al. (2013) proposed that models using a higher-than-observed lateral eddy
8 diffusion coefficient (Aredi) simulate a higher diffusive flux of O₂ from the west along the
9 equatorial Pacific, thereby reducing the modeled OMZ volume. However, our comparison
10 showed no correlation between the reported Aredi coefficients (Table A2) and Pacific OMZ
11 volumes across CMIP5 models. This suggests that either model differences are not primarily
12 due to lateral mixing or, more likely, that it is not possible from this set of models alone to
13 distinguish the effect of mixing from other parameters in the system. In particular, of the two
14 models with the largest Aredi (1000 m/s²), IPSL-CM5A agrees with the expectation showing
15 low subsurface anoxia, but MPI-ESM models disagrees with the expectation by displaying
16 large OMZ.

17

18 *Inadequate representation of diapycnal mixing*

19 Duteil and Oschlies (2011) found that OMZ were progressively smaller at low and large
20 background vertical diapycnal diffusivity coefficient K_v (above and below $K_v = 0.2 \text{ cm}^2/\text{s}$). At
21 high diffusivities, the OMZs are well ventilated. At low diffusivities, the OMZs are not well
22 ventilated but the consumption of oxygen is low because there is not much biological activity.
23 Only at intermediate coefficients, the OMZs are large due to high consumption combined with
24 relatively low ventilation. Among CMIP5 models, MPI-ESM, IPSL-CM5A, and GFDL-
25 ESM2M assume a background value of $K_v = 0.1 \text{ cm}^2/\text{s}$ in the tropics, while models CESM1-
26 BGC, NorESM1-ME, HadGEM2, and GFDL-ESM2G assume a value of $K_v = 0.01 \text{ cm}^2/\text{s}$.
27 According to the findings by Duteil and Oschlies (2011), the former three models should have
28 a larger OMZ compared to the last four models. However, we do not see this expected
29 tendency across CMIP5 models.

30

3.1.2 Biological causes for OMZ biases in historical simulations

The main biological drivers of biases in the simulation of OMZs are biases in the export of particulate organic carbon (POC) at 100-m depth, the transfer efficiency of POC from 100m to depth (defined as the POC export at a given depth divided by POC export at 100m) and the way POC is treated at the sea floor (Kriest et al. 2010, 2012). We also considered the effect of the variability in models' O₂:nutrient ratios since these ranges from 150 to 172 (in the case of the O₂:P ratio). However, we could not find any direct correlation with OMZ biases.

Finally, we considered the effect of DOC variability across models. The range of observed DOC in the low latitude Pacific is 65-80 mmol/m³ in the upper 200m, decreasing with depth to background concentrations of less than 40 mmol/m³ below 1000m (Hansell, 2013). The CMIP5 models that reported DOC (all models but HadGEM2) show very diverse ranges of concentrations but in general they underestimate the observed values by 20 to 55 mmol/m³ in the upper 200m. Exceptions are the GFDL-ESM2 models that have realistic vertical distributions of DOC at low latitudes. In order to achieve the right distribution of DOC, models should have at least two DOC compartments (as only GFDL-ESM2 models do), one labile and one refractory. Most of the DOC in the ocean is in a refractory or unavailable form with estimated turnover timescales of centuries to millennia (Hansell, 2013), while the remaining DOC is in a labile and reactive form with short turnover timescales. Higher concentrations of dissolved organic matter, in general, allow for nutrient export out of the production region, decreasing the local consumption of oxygen. However, we do not see any correlation between levels of DOC and hypoxia in CMIP5 models. For example, the GFDL models, with a good representation of DOC, show more hypoxia than most models that underestimate DOC.

Biased export of POC at 100m depth

A deep OMZ could be caused by an anomalously high POC flux at 100-m depth, which in turn can be due to excessive primary productivity, excessive nitrogen fixation by diazotrophs, or excessive relative abundance of large phytoplankton, which are major contributors to sinking POC. For the CESM1 model, Moore et al. (2007) found that simulated POC export in the Pacific is primarily driven by upwelling (nutrient supply) and less by nitrogen fixation,

1 suggesting that the model representation of diazotrophs probably does not affect the level of
2 anoxia in this model and probably in the rest of models with similar biogeochemistry (Table
3 A3).

4 In order to quantify model biases, we considered three different POC export observational
5 estimates for our area of study (20°S to 20°N and 180°E to 60°W in the Pacific Ocean). We
6 compare these database estimates with our modeled POC in Fig. 5 (See Sup. Fig. S1 for a map
7 of export fluxes). When compared to satellite-derived estimates based on sediment traps and
8 thorium (Dunne et al., 2005) or estimates from satellite observations combined with food-web
9 models (Siegel et al., 2014), at least four models predict too high values of POC flux
10 (assuming errors of 35% in Dunne et al., 2005 and 20% in Siegel et al., 2014 as reported).
11 However, all CMIP5 models predict POC values significantly above thorium-derived satellite
12 estimates by Henson et al. (2012). An overestimate of export at 100 m depth contributes to
13 anomalously deep OMZ in the MPI-ESM and NorESM1-ME models. GFDL-ESM2M and
14 GFDL-ESM2G, with POC flux at 100-m depth consistent with observations, still develop a
15 deep OMZ, probably due to a biased transfer of POC to depth, as discussed next. MRI-ESM1
16 overestimates the sinking POC flux from the surface and hence overestimates remineralized
17 nitrate throughout the water column (Fig 3c), but attains realistic oxygen levels by
18 remineralizing a high proportion of the organic matter near the surface. The remaining models
19 predict POC flux values in accordance to Dunne et al. (2005) and Siegel et al. (2014).

20

21 *Biased transfer efficiency of POC from 100m to depth*

22 A too large transfer of POC flux from upper layers to deeper layers would cause
23 remineralization to occur too deeply, hence leading to phosphate trapping and too much
24 oxygen and nitrate consumption in the deep ocean. Therefore, most remineralization should
25 ideally take place right below the euphotic zone in order to avoid the formation of too deep
26 OMZs.

27 Thorium-derived POC export and POC flux to deep-sea sediment traps (Henson et al., 2012)
28 indicate that the transfer efficiency of POC from the euphotic (100m) to deeper layers is
29 higher at low latitudes than high latitudes (Supp. Fig. S2). However, newer measurements
30 using neutrally buoyant sediment traps at intermediate depths suggest a correlation between
31 high temperature and high remineralization, resulting in low transfer efficiency of POC to
32 intermediate depth at low latitudes or high temperatures (Marsay et al., 2014). The

1 discrepancies in these two observational results are due to data sparseness and measurements
2 coming from different depths. This suggests that the POC profiles should not only be fitted
3 with power laws or exponentials as traditionally done, but with a more sophisticated
4 combination of these (Marsay et al., 2014).

5 The CMIP5 models use either a sum of exponential or power-law expressions to represent the
6 vertical flux of particulate organic matter (Fig. 6 and equations in Table A3) but do not yet
7 capture the observed latitudinal variability (Supp. Fig. S2). In models where detritus is not
8 represented explicitly, a large transfer of POC flux from upper layers to deeper layers is
9 equivalent to a slow decrease of POC flux with depth and a low exponent in the Martin's
10 power-law curve (Martin et al. 1987). Models with explicit detritus representation would
11 replicate this effect by either using a too-high sinking speed or a too-low remineralization rate
12 (see Table A3). For example, IPSL-CM5A-MR prescribes an approximate power law with a
13 lower exponent (higher transfer efficiency) than HadGEM2-ES (Fig. 6c-d). Exponential
14 curves would also create a large POC transfer from subsurface to intermediate depths as the
15 curvature of the depth profile at 100-300m is usually lower than for power-law profiles with
16 exponents between 0.8-0.9 (typical profiles according to Martin et al. 1987). This low
17 subsurface POC remineralization (large transfer) combined with a sudden increase in the POC
18 remineralization (low transfer) at intermediate depths (300-800m) results in stronger-than-
19 observed remineralization in the low oxygen part of the column, forcing anomalous formation
20 and extension of OMZs (for example, see the CESM1-BGC POC sinking profile in Fig. 6b).
21 In conclusion, in order to match the observed oxygen concentrations, we propose that a
22 Martin's exponent higher than typically observed values and a power law (instead of
23 exponential) are preferable, as they ensure large remineralization rates in the upper layers and
24 thus reduce anomalously high transfer of POC and oxygen consumption at depth. This agrees
25 with findings from Kriest et al. (2010) based on sensitivity studies to the remineralization
26 curve.

27 According to these expectations, the CMIP5 models with exponential profiles usually produce
28 deeper oxygen consumption associated with respiration than the models that use a power law
29 (Fig. 6 and Table A3). NorESM1-ME and MPI-ESM both show an exponential profile and
30 show similarly deep OMZ (Fig. 6a). These models share the same biogeochemical module
31 HAMOCC and differ in the representation of physical processes, suggesting that indeed their

1 exponential parameterization of the remineralization curve is the cause for the deep OMZ.
2 The GFDL-ESM2 models, with deep OMZs, also use an exponential profile (Fig. 6a).

3 In the subsurface, extensive denitrification worsens the problem of low-oxygen biases at
4 depth. Models typically have an oxygen cutoff for respiration – discussed in Table A2 –
5 below which denitrification remineralizes organic matter by consuming nitrate instead of
6 oxygen. The length scale of remineralization is usually larger in denitrification than in oxic
7 remineralization, pushing POC deeper in the water column and hence causing the OMZs to
8 extend deeper than under oxic remineralization. Even though the remineralization length-scale
9 (and thus oxygen consumption) is similar between HAMOCC and TOPAZ (biogeochemical
10 module for GFDL-ESM2 models) – 200 m and 187.5 m respectively - the length scale of
11 denitrification is considerably larger in TOPAZ (1500 m) compared to HAMOCC (1000 m).
12 This leads to POC being transported deeper in GFDL-ESM2 models compared to the
13 NorESM1-ME and MPI-ESM models (also see Dunne et al., 2012). Additionally, the
14 inclusion of ballast terms (Armstrong et al., 2002) in TOPAZ contributes to increase further
15 the transfer of POC to depth.

16
17 The model CESM1-BGC does not develop a deep OMZ despite using an exponential curve
18 (Fig. 6b, Fig. 2), similar remineralization parameters and ballast terms to GFDL-ESM2
19 models, partly because the denitrification length scale is much lower than in GFDL-ESM2
20 (260m compared to 1500m). **Additionally, the CESM1-BGC model adjusts the nitrate
21 consumed during denitrification to lower values to avoid running out of nitrate (Lindsay et al.,
22 2014), which might suppress the transfer of POC to depth, and hence the expansion of OMZ
23 to depth.** MRI-ESM1, also with an exponential profile (Fig. 6a), does not develop deep OMZ
24 due to a very low transfer of POC to depth (large exponent in Table A3), which facilitates
25 consumption in the upper ocean. Even though MRI-ESM1 thus solves the deep anoxia
26 problem, the shallow modeled nitrate and POC export are higher than observed possibly due
27 to too fast recycling of organic matter near the surface (Fig. 3c).

28 Only two models use a power law as a remineralization profile. The HadGEM2 models, with
29 an exponent power law as in Martin curve (Fig. 6c) and no denitrification, do not develop a
30 deep OMZ as expected. While in theory a power law is preferable to an exponential, the
31 IPSL-CM5A models uses a very low exponent (relative to the Martin curve, Fig. 6d and Supp.
32 Fig. S2), resulting in a high transfer of POC to depth, which explains the positive oxygen

1 anomalies in subsurface layers and contributes together with a lack of deep ventilation to a
2 deep hypoxic region (Fig. 2).

3

4 *Treatment of POC at the sea floor*

5 If models bury a fraction of POC into the sediments when reaching the sea floor, the
6 sensitivity of oxygen consumption to POC profile is reduced (Kriest and Oschlies, 2013). In
7 the opposite case, if POC is remineralized back to the water column when hitting the floor, it
8 could enlarge considerably the OMZ in models with high deep POC flux. NorESM1-ME and
9 MPI-ESM are the only models that include a full sediment module such that part of the POC
10 reaching sediments becomes unavailable to remineralization at each time step (Table A3). In
11 IPSL-CM5A models, sinking organic matter is permanently buried below the sea floor, where
12 it is not subject to remineralization. Hence, the low levels of oxygen in this model are more
13 likely attributed to ventilation deficiencies. The rest of the models remineralize the remaining
14 POC back to the water column when reaching the sea floor (Table A3).

15 The impacts of sediment scheme differences are most noticeable among models with low
16 oxygen and high POC at depth. While the tropical OMZ reaches the bottom in GFDL-ESM2
17 models (consistent with no sediment scheme and instant remineralization), the OMZ does not
18 reach the bottom in the NorESM1-ME and MPI-ESM models (consistent with partial organic
19 matter burial in sediments). We do not observe any impact of sediment scheme on the depth-
20 distribution of OMZs in other models.

21 **3.1.3 Suggestions for improving the representation of OMZs in models**

22 The ultimate question is what proportions of the excessive OMZ volume are due to equatorial
23 zonal ventilation, mid-depth ventilation (from AAIW, SAMW and NPIW) and local
24 consumption (remineralization), respectively. We agree with previous studies (Stramma et al.,
25 2010a; Dietze and Loeptien, 2013; Montes et al., 2014) that an accurate description of local
26 equatorial ventilation in the Pacific Ocean would help reduce the large modeled volume of
27 OMZs by providing additional channels for the supply of oxygen-rich waters and the removal
28 of low-oxygen and nutrient-loaded waters. This requires a **very** high resolution for improving
29 the representation of all the equatorial jets **or alternatively a parametrization of intermediate**
30 **jets, for example by using anisotropic diffusion coefficients (Getzlaff and Dietze, 2013).**
31 Correct lateral ventilation from the Southern Ocean and North Pacific is also important for the

1 correct characterization of OMZs, stressing the need to solve the insufficient flow of
2 AAIW/SAMW and the often-exaggerated deep North Pacific ventilation via NPIW or via
3 AABW as discussed in section 3.1.1 (Fig. 2). With more realistic equatorial ventilation, the
4 depth of the OMZs would probably be less sensitive to slight changes in POC profiles, as
5 most remineralization would happen in the upper ocean without the need to switch so
6 extensively to denitrification, which in turn causes the OMZs to extend more deeply. On the
7 other hand, reduction in the POC flux leaving the euphotic layer and a shallower
8 remineralization achieved by using a power-law curve with low transfer of POC to depth, or a
9 large denitrification rate, would improve the representation of the OMZs even before the
10 representation of equatorial ventilation is improved. Additionally, the inclusion of a sediments
11 module that does not prescribe instantaneous consumption of all the POC that reaches the sea
12 floor but instead involves partial burial might alleviate the anomalously deep OMZ.

13 **3.1.4 Overlap between observed and modeled OMZs**

14 In order to evaluate the performance of CMIP5 models regarding their representation of
15 OMZs in the tropical Pacific, we introduce a metric aimed at identifying the spatial overlap
16 between observed and modeled OMZ (Fig. 7 and Supp. Fig. S3). The metric is calculated by
17 finding, for a given oxygen threshold, the volume that results from the intersection of modeled
18 and observed OMZ, and dividing it by the volume that results from the union of modeled and
19 observed OMZs. A metric value equal to 1 means that modeled and observed OMZs occupy
20 the same exact volume, while a value close or equal to 0 signifies a lack of intersection or/and
21 a large difference in area extension between the modeled and observed OMZs. This metric
22 penalizes models that misplace the OMZs compared to observations or models that enclose
23 the observed OMZ area/volume but overestimate the OMZ extent.

24 Generally, the models are not capable of successfully representing anoxic zones ($O_2 < 10$
25 mmol/m^3), but show gradual improvement as O_2 concentration thresholds increase (Fig. 7a).
26 As oxygen thresholds are progressively increased from 10 to 100 mmol/m^3 , CESM1-BGC is
27 always found to be closest to observations everywhere in the tropical Pacific (Fig. 7 and Supp.
28 Fig. S3). While its overlap metric value is only 0.2 at $O_2 < 10 \text{ mmol/m}^3$ it markedly improves
29 to 0.7 when the threshold O_2 is set to 100 mmol/m^3 . Another model that is close to
30 observations in the North Pacific is MPI-ESM (Supp. Fig. S3). In the South Pacific, both
31 CESM1-BGC and MRI-ESM1 reproduce the observations fairly well, followed by HadGEM2
32 (Supp. Fig. S3). Importantly, in the surface layers (depth range from 0 m to 400 m), most

1 models perform similarly, reaching an overlap metric of about 0.6 at hypoxic concentrations
2 ($O_2 < 60\text{-}80 \text{ mmol/m}^3$), with the exception of IPSL-CM5A and HadGEM2-ES with
3 substantially lower overlap metric values (Sup. Fig. S3). Panels b) and c) in Fig. 7 show in
4 detail model performance at each depth when OMZs are defined with O_2 threshold of 50
5 mmol/m^3 . Panel b) shows once more that some models predict too deep OMZs. Most models
6 reproduce well the depth at which the northern OMZ is largest, around 1000m, despite the
7 dispersion in OMZ area across models. However, in the SH, most models predict the largest
8 OMZ to be deeper than observed. Most models achieve the best overlap metric at 300m depth
9 in the SH and 500m depth in the NH and progressively fail to reproduce the OMZs at
10 shallower and deeper depths (Fig. 7c). Similar conclusions apply when other oxygen
11 thresholds are considered.

12 **3.2 Oxygen changes in the Pacific from 1990 to 2090**

13 In this section we present changes in oxygen concentrations and the extent of OMZs in the
14 Pacific throughout the 21st century, as well as the mechanisms responsible for those changes.
15 **We also explore how the biases found across CMIP5 models in the mean state (Section 3.1)**
16 **propagate into 100-year timescale changes.** Global changes in oxygen concentrations are
17 summarized in Table 1 for all the CMIP5 models. Changes in O_2 can be due to either changes
18 in AOU or changes in $O_2\text{sat}$:

$$19 \quad \Delta O_2 = \Delta O_2\text{sat} - \Delta \text{AOU}$$

20 We find that on average across all CMIP5 models, oxygen decreases around 3% globally by
21 the end of the 21st century (in agreement with Bopp et al., 2013). This drop is due to both
22 global average decreases in $O_2\text{sat}$ and increases in AOU, with similar contributions from each
23 in the multi-model mean (Table 1). The drop in oxygen originally stems from high latitudes
24 and deep oceans (Fig. 8c), and is due to a combination of $O_2\text{sat}$ decreases (Fig. 8f) and AOU
25 increases (Fig. 8i). As expected, the thermal contribution (via $\Delta O_2\text{sat}$) to the global oxygen
26 decrease (ΔO_2) was lower, around 25-50%, in the previous Coupled Model Intercomparison
27 (CMIP3) under the SRESA2 scenario (with less overall warming than RCP8.5), while the rest
28 was ascribed to changes in oceanic ventilation (e.g. Table 2 in Keeling et al., 2010). Historical
29 measurements from the 1970s to the 1990s already reflect these long-term predictions (Helm
30 et al., 2011).

1 Next we discuss centennial changes in oxygen across different regions. In Fig. 8 we show for
2 O₂, O₂sat, AOU, and water-mass age a meridional section of the eastern Pacific. The historical
3 observed values together with the historical multi-model averages are shown in Fig. 8 in
4 reference to Section 3.1. The last column of Fig. 8 shows the multi-model averaged centennial
5 changes and the consistency of the predicted trends across models (for individual model
6 projections see Sup. Fig. S4, S5, and S6). Fig. 10a (described later) shows a schematic of the
7 regions of interest described in the following text.

8

9 *Zones of subduction and propagation of deep water masses:*

10 Surface freshening and warming south of 60°S were shown to result in a weakening of
11 AABW formation over the 21st century for IPCC AR4 models (Sen Gupta et al., 2009).
12 Additionally, warming and freshening in the formation zones of mode and intermediate water
13 masses (Sallee et al., 2013a) results in a reduced ventilation of Southern Ocean intermediate
14 layers across CMIP5 models under the RCP8.5 scenario (Sallee et al., 2013b), as also
15 observed by Downes et al. (2010) across IPCC AR4 models under the SRESA2 emissions
16 scenario. Meijers et al. (2014) provides a complete review of water masses transformation
17 under climate change across CMIP5 models.

18 The usual expectation is that for a given water-mass, the older the age the more time there is
19 for organic matter and oxygen to be consumed, hence the higher the AOU, and the lower the
20 O₂ in the water sample. This relationship holds well over most of the deep ocean on
21 interannual time scales, as seen by the positive correlation between age and AOU in Sup. Fig.
22 S7a and the negative correlation between AOU and O₂ in Sup. Fig. S7b. This relationship also
23 holds well on centennial timescales. We see that, over the 21st century, climate-driven
24 decreases in deep ocean ventilation along the AABW in the Southern Ocean and along the
25 NPIW in the North Pacific increase age (Fig. 8l) and increase AOU (Fig. 8i), contributing to a
26 decrease in O₂ along these ventilation pathways (Fig. 8c). The patterns of increased AOU and
27 decreased oxygen can also be seen in individual model projections (Sup. Fig. S4 and S5).

28 However, the expected relationship between water-mass age and AOU is opposite from
29 expectations in the deep North Pacific in the NorESM1-ME and GFDL-ESM2G models, i.e.
30 decreased ventilation (Sup. Fig. S6) is accompanied by decreased AOU (Sup. Fig. S5).
31 Interestingly, the same mechanism that controls the relation between age and AOU
32 interannually controls the 100-year time changes in the 4 models that include age tracers (not

1 shown). The deep North Pacific is the least ventilated basin, such that isopycnal ventilation is
2 weak there and the diapycnal supply of oxygen gains importance (Karstensen et al., 2008),
3 which could contribute to the age-AOU disagreement. **Moreover, with climate change, the**
4 **percentage of saturated O₂ could increase, which then would increase the input of oxygen into**
5 **the ocean interior, ultimately decreasing the estimated AOU (that assumes O₂ to be 100%**
6 **saturated at the surface) even if respiration increased (Bernardello et al., 2014).** As a result of
7 decreased AOU in the North Pacific, AOU does not increase as much globally in NorESM1-
8 ME compared to other models. Therefore, this model experiences a lower decrease in global
9 O₂ (1.3%) over the 21st century, mostly driven by the contribution of O₂sat decrease (82% in
10 Table 1) with little contribution from AOU increase, contrary to the rest of models (Table 1).

11 O₂sat decreases in zones of deep water-mass formation (Fig. 8f) due to 21st century warming,
12 contributing (together with the increase in AOU) to the decrease in oxygen levels **in deep**
13 **waters**. Note that AOU and O₂sat are anti-correlated in zones of deep water subduction on
14 both centennial and interannual scales as decreased ventilation (and hence increased AOU) is
15 usually associated with warmer waters (and lower O₂sat) (Sup. Fig. S7d).

16

17 *Upper Ocean (top 100m):*

18 In the upper ocean above the thermocline, O₂sat drops significantly everywhere as
19 temperature increases (Fig. 8f), acting to decrease O₂ (Fig. 8c). O₂sat dominates the changes
20 in O₂ on both the 100-yr time scale and the interannual scales (Sup. Fig. S7c). The exception
21 to this are the low-oxygen sub-surface eastern zones where O₂ is predicted to increase over the
22 21st century following a strong decrease in local AOU, higher than the warming-induced
23 decrease in O₂sat.

24 This decrease in AOU results from both a strong stratification-driven decrease in nutrient
25 supply and reduced mixing with old high-AOU waters under future warming.

26

27 *Low-latitude intermediate depths (200-1000m):*

28 At low-latitude intermediate depths, the changes in oxygen levels over the 21st century are
29 small in the multi-model mean (Fig. 8c) owing to a strong compensation between decreased
30 AOU and decreased O₂sat (reduced solubility). The **decreasing** trends in both AOU and O₂sat
31 are consistent across models **in the most central part of this region** (Fig. 8f and 8i). Increased

1 stratification reduces the supply of nutrients to the euphotic zone, acting to reduce
2 productivity and consumption of oxygen (AOU decrease) especially in the eastern highly
3 productive tropics. However, changes in ventilation (as tracked by the water-mass age)
4 explain most of the decrease in AOU outside the eastern anoxic regions (Fig. 8l). Both water-
5 mass age and AOU drop due to a decrease in the upward transport of old, high AOU deep
6 waters (Fig. 8h,k) following increased stratification (Gnanadesikan et al. 2007, Gnanadesikan
7 et al. 2012). The oxygen trend is highly inconsistent across models, as seen in Fig. 8c (no
8 patterns). Inter-model discrepancies in predicted trends result from the strong compensation
9 between decreased O_2 sat and increased AOU and from slight differences across models in the
10 exact location of this poorly ventilated region (Sup. Fig. S4). The finding that the multi-model
11 mean change in O_2 is not significant agrees with previous model studies (Cocco et al. 2013;
12 Bopp et al. 2013 across CMIP5 models).

13 As oxygen remains approximately constant with climate warming in mid-depth tropics, 21st
14 century changes in tropical OMZ volume are small in most CMIP5 models (Fig. 9 and Sup.
15 Fig. S8). In anoxic regions ($O_2 < 5 \text{ mmol/m}^3$) CMIP5 models show an increase or decrease in
16 volume (by about 10%) depending on the balance between O_2 sat and AOU contributions and
17 changes are indistinguishable from natural variability for GFDL models. Changes in the
18 volume of anoxic regions are of critical importance for the survival of organisms and for
19 denitrification, which occurs at low oxygen values. However, the skill of models in
20 representing anoxic regions is poor (Fig. 7a), so this result should be taken with caution. The
21 volumes of hypoxic regions ($O_2 < 80 \text{ mmol/m}^3$) mostly increase, although slightly, due to
22 decreased overall ventilation and increased AOU. Hypoxic volumes encapsulate wider regions
23 than anoxic regions, so these are not dominated anymore by local consumption but by overall
24 ventilation. As an exception, IPSL-CM5A predicts an increase of both anoxia and hypoxia
25 (this model can only be seen in Sup. Fig. S8), as changes in oxygen levels are dominated by
26 decreased ventilation even within anoxic regions. CESM1-BGC similarly predicts an increase
27 in OMZ volume everywhere driven by changes in ventilation at intermediate depths (500-
28 1000m). The anomalously high interannual variability in HadGEM2 in anoxic regions is due
29 to a small OMZ size, which artificially boosts the relative changes.

30

31 *Summary:*

1 In accordance to the regimes just explained, we identify three zones in the Pacific Ocean with
2 similar properties: (i) surface layers, (ii) deep Pacific and high-latitude intermediate depths
3 (coinciding with the multi-model increase in age in Fig. 8l), and (iii) low-latitude intermediate
4 depths (coinciding with the multi-model decrease in age in Fig. 8l). Fig. 10 shows trends in
5 O_2 , O_{2sat} , and AOU across CMIP5 models separated into (a) surface box (50 to 200 m), (b)
6 intermediate box (200 to 1000 m), and (c) deep box (2000 to 4000 m). Surface O_2 is predicted
7 to decrease in all the models due to warming-driven O_{2sat} decrease (Fig. 10a). In the deep
8 Pacific, most models show a decrease in oxygen levels, due to reduced ventilation (increased
9 water-mass age) - increase in AOU - and due to increased temperature - decrease in O_{2sat}
10 (Fig. 10c). Similarly, high-latitude intermediate depths (between 200 m and 1000 m) in the
11 zones of water-mass formation are expected to experience decreases in oxygen concentrations
12 (shown in blue in Fig. 10b) due to decreased ventilation, as in the deep box, coinciding with
13 the multi-model increase in age in Fig. 8 l. Only at the low-latitude intermediate depths (OMZ
14 region, red in Fig. 10b), where AOU mostly decreases due to reduced mixing with old waters,
15 oxygen levels are predicted to remain nearly constant (i.e. to increase or decrease only
16 slightly, depending on the model) due to a high-degree of compensation between changes in
17 O_{2sat} and AOU (Fig. 10b). Importantly, the same physical regions can be analyzed on
18 interannual time scales (Sup. Fig. S7). Surface oxygen is dominated by changes in O_{2sat}
19 (Supp. Fig. S7b) and deep and high-latitudes oxygen is dominated by changes in AOU (Sup.
20 Fig. S7b) which is in turn very correlated to changes in age (Sup. Fig. S7a). Low-latitude
21 intermediate oxygen changes result from a compensation between increased O_{2sat} and
22 decreased AOU (or opposite) as seen in Supp. Fig. S7d and discussed in next section.

23 **It is worth noting that we found no correlation between biases in the mean state and responses**
24 **to climate change, suggesting that the mechanisms underlying the change are similar and**
25 **robust in all models.**

26 **3.3 Oxygen dynamics in the eastern tropical Pacific OMZ: Interannual** 27 **variability compared to long-term changes**

28 The most interesting dynamics in the oxygen system is the strong compensation between
29 AOU and O_{2sat} through the 21st century below the thermocline in the eastern tropical Pacific
30 (Fig. 8c,f,i). In this section we highlight the mechanisms controlling oxygen variations on
31 both interannual and long-term timescales between 10°S and 10°N and east of 115°W, at a
32 depth of 100 to 200m. This domain is chosen to enclose the upper portion of the eastern

1 tropical Pacific OMZ, found to have interesting oxygen dynamics due to the strong
2 compensation between AOU and O_2 sat through the 21st century (Section 3.2, Fig. 8c,f,i). We
3 explore here the same compensation mechanisms discussed in Section 3.2 but on interannual
4 timescales. This region is also of interest because tropical oxygen is underestimated in many
5 CMIP5 models compared to observations (Fig. 3a), since models do not properly separate the
6 northern and southern OMZs (Fig. 1) as explained in Section 3.1.

7 The temporal evolution of the system is shown in Fig. 11 both for interannual variability
8 (ellipses) and for long-time trends (wiggly lines) across CMIP5 models. For each model, the
9 ellipses encapsulate 95% of the interannual variability calculated in the 100-year control time
10 series.

11 On interannual scales, the oxygen concentration in this eastern Pacific region depends on the
12 compensating effects between increased O_2 sat and increased AOU (Fig. 11a), which are
13 highly correlated since both are forced by changes in Walker circulation (Fig. 11b-c). During
14 years with strong upwelling (coinciding with 'La Niña' events or strong Walker circulation)
15 the thermocline shallows in the East Pacific. An increased zonal tilting of isopycnals brings
16 more nutrients to the surface increasing photosynthesis, local remineralization and AOU and
17 acting to decrease O_2 . Additionally, increased Walker circulation is also associated to
18 increased inflow of deep water, which is not well ventilated and thus contains high levels of
19 accumulated AOU, also acting to decrease O_2 in the OMZ region. At the same time, the
20 upwelling of cold deep waters results in a temperature-driven increase in oxygen solubility
21 (O_2 sat) and thus an increase of O_2 .

22 On interannual scales, all the models predict O_2 changes dominated by AOU changes, shown
23 by the slopes of the ellipses in the O_2 sat-AOU relation in Fig. 11a. Hence, a strong Walker
24 circulation results in increased O_2 . The variability in O_2 sat, controlled by physical
25 mechanisms only, is more tightly related than AOU to changes in Walker circulation (less
26 dispersion in ellipses in Fig.11b vs 11c) at all depths. A more detailed analysis shows that
27 changes in AOU are due to local remineralization at 100 m but become gradually more
28 dominated by changes in water-mass age at 200 m and below. These considerations apply to
29 the whole suite of CMIP5 models, and support results from the hindcast model by Ito and
30 Deutsch (2013). It is worth noting that most models overestimate O_2 sat compared to
31 observations (cross in Fig. 11) due to the well-known cold bias in the tropics (Lie and Xie,
32 2014). AOU is also overestimated in seven models, because of the nutrient trapping problem

1 discussed in Section 3.1.2. However, the strength of the modeled Walker circulation and its
2 natural variability is similar to the observed one (Fig. 2b-c) except for GFDL-ESM2M, which
3 overestimates Walker circulation variability.

4 The centennial behavior is illustrated by the AOU, O₂sat, Walker and stratification index
5 trajectories from 1900 to 2099 (wiggly solid line in Fig. 11a-e). The 100-year trend in Walker
6 circulation strength is low and discrepant across the CMIP5 ensemble (Fig. 11b wiggly lines),
7 although most models show a slight decrease of its strength (Sandeep et al. 2014 and
8 reference therein). However, the eastern tropical Pacific in CMIP5 models stratifies mainly
9 due to increased warming and increased precipitation (Cabr e et al., 2014) and not due to
10 centennial changes in Walker circulation strength. As a consequence, less cold, old and
11 nutrient-rich waters are upwelled and mixed from deeper layers as explained in Section 3.2.
12 The consequent decrease in surface productivity and in water age results in less local and
13 accumulated oxygen consumption via remineralization (less AOU) across all models (Fig.
14 11d). Additionally, O₂sat gradually decreases across all models as a result of reduced inflow
15 of cold-deep waters and overall increase in ocean temperatures (Fig. 11e). Note that while we
16 define here stratification as the density difference between 200m and surface, analysis of other
17 variables depicting changes in density structure such as thermocline depth show similar
18 results.

19 The centennial behavior of the system (wiggly lines) is different from the interannual
20 variability (ellipses). Although the sensitivity to changes in stratification for O₂sat is the same
21 for interannual and 100-year time scale (Fig. 11e ellipse slope similar to 100-year trend
22 slope), the sensitivity to changes in stratification for AOU is larger for interannual compared
23 to the centennial timescale (Fig. 11d ellipse slope larger than 100-year trend slope). As a
24 result, the reduction of O₂sat relative to the reduction in AOU is more pronounced on the 100-
25 year timescale than on the interannual timescales (Fig. 11a). Graphically, this means that the
26 O₂ centennial wiggly line in Fig. 11a becomes more parallel to the constant O₂ lines compared
27 to the ellipse slope. Thus, on the 100-year time scale there is almost perfect compensation
28 between the AOU and O₂sat such that O₂ does not change significantly across the CMIP5
29 models. By contrast, AOU changes dominate O₂sat changes, resulting in more significant
30 changes in O₂ on the interannual timescales. We hypothesize that this differential behavior at
31 different time scales is due to the fact that increased stratification with climate change moves
32 the isopycnals deeper, changing the relative importance of lateral over vertical mixing.

1 Moreover, we hypothesize that the local biological positive feedback, very important at
2 interannual scales for AOU changes, is dampened at longer time scales as the system adjusts
3 the new levels of physical nutrient supply.

4

5 **4 Conclusions**

6 Here we studied the differences in contemporary and 21st century oxygen distributions across
7 the latest generation of Earth System Models CMIP5 in the Pacific Ocean. The range of
8 physical and biogeochemical characteristics across CMIP5 models offers a unique opportunity
9 to understand common and persistent mechanisms and biases.

10 We find that the volume of OMZs is systematically overestimated across CMIP5 models in
11 agreement with previous work (e.g. Bopp et al., 2013), largely because of overestimated
12 weakening of the Equatorial Under Current on the Eastern side, too weak surface
13 countercurrents, and lack or deficiency of deeper equatorial jets. The biases in equatorial
14 ventilation combined with large biological consumption result in strong oxygen depletion,
15 phosphate trapping at depth, and (often) too low nitrate due to excessive denitrification (Fig.
16 3). Consequently, most models tend to join the northern and southern OMZ cells – well
17 separated in observations – into a single large tropical OMZ (Fig. 1a).

18 The southern Pacific OMZs are found to be too large compared to observations, as
19 intermediate water ventilation from the Southern Ocean does not reach sufficiently north in
20 the Pacific (in agreement with Sallee et al., 2013b and Downes et al., 2010). Some models
21 additionally predict positive biases in oxygen concentrations at the northward edge of the
22 northern OMZ, due to excessive NPIW transport and excessive deep ventilation from AABW
23 towards the North Pacific. This creates a meridional distribution of oxygen that is too
24 symmetric across the equator compared to observations (Fig. 1).

25 The POC flux at 100m is significantly larger than observations across at least four CMIP5
26 models, triggering excessive oxygen consumption. The OMZ expands too deep for models
27 with low remineralization in the upper ocean, associated with a high transfer of POC to depth.
28 We find that a power law POC remineralization profile with large shallow remineralization
29 and low transfer of POC to the deep matches better the observed oxygen concentrations.

30 With realistic equatorial ventilation, the depth of the OMZ would probably be less sensitive to
31 changes in POC profiles because it would not switch from aerobic remineralization to

1 **denitrification** so easily, but until the representation of equatorial ventilation is improved, a
2 higher exponent in POC transfer power-law curve, and higher denitrification rates might
3 alleviate the anomalously deep OMZ. **We recommend the calibration and examination of**
4 **sediment models**, since the lack of sediments burial at the sea floor might contribute to
5 anomalously deep OMZ if all the remaining POC is remineralized instantaneously at the sea
6 floor.

7 Complexity in the representation of biogeochemistry does not seem an advantage in modeling
8 OMZs within this generation of coarse resolution simulations. The most complex
9 biogeochemical models (CESM1-BGC, GFDL-ESM2, and IPSL-CM5A), with ballast or size
10 dependent remineralization and denitrification - display OMZ biases similar to the rest of the
11 models. We provide summary tables of ocean physics (Table A2) and biological
12 representations and parameters (Table A3) for all the CMIP5 models analyzed. These tables
13 complemented with recommendations in Section 3.1.3 will be useful for modelers who want
14 to improve the representation of OMZs, and of the processes that control them. Furthermore,
15 we created the overlap metric described in Section 3.1.4 to help select models with the least
16 OMZ biases compared to observations for biogeochemical studies.

17 Under typical climate change scenarios, all CMIP5 models predict similar deoxygenation
18 mechanisms during the 21st century, despite large differences in the oxygen mean state. The
19 consistency with which the different models predict changes in O₂sat and AOU suggests that
20 the mechanisms underlying the change are similar and robust across all models and that biases
21 in the mean state do not affect the expected response to climate change.

22 CMIP5 models predict a decrease of oxygen over most of the deep and high latitudes ocean
23 due to overall slow-down of ventilation (increased AOU) and increased temperature
24 (increased O₂sat), in agreement with observed decreasing trends in deep O₂ over recent
25 decades (Helm et al. 2011). Consistency among model predictions (Fig. 8c) and agreement
26 with recent observed trends at high latitudes suggests that this is a robust mechanism that we
27 should continue to monitor with future biogeochemical observing systems. We also find
28 coherent patterns of oxygen **trends** with climate change in the Pacific surface (section 3.2, Fig.
29 10a), where oxygen decreases due to warming (O₂sat decrease).

30 The most complex behavior is displayed in the intermediate tropical depths where the OMZs
31 reside. On interannual time scales, we find that both changes in O₂sat and AOU there are
32 systematically connected to the Walker circulation and ENSO variability across all CMIP5

1 models, as previously observed in the southern tropical Pacific (Llanillo et al. 2013) and
2 discussed in a single hindcast model by Ito and Deutsch (2013). The interannual variability of
3 the upper part of the tropical Pacific OMZ is dominated by changes in AOU over changes in
4 O₂sat, such that years with strong Walker circulation are years of increased AOU and lower
5 total oxygen.

6 In contrast to interannual variability, CMIP5 models project AOU increases and O₂sat
7 decreases that almost compensate over the 21st century, such that climate-driven predictions in
8 tropical mid-depth oxygen are consistent with no oxygen change across the CMIP5 models.
9 This agrees with predictions from previous modeling studies (Bopp et al. 2002, Matear and
10 Hirst, 2003; Cocco et al., 2013; Bopp et al., 2013). The projected AOU decreases in the
11 eastern tropical mid-depths throughout the 21st century are due to increased stratification and
12 hence a) less advection of deep, AOU-rich waters and b) decreases in biological production;
13 the projected O₂sat decreases are due to warming.

14 However, observations have shown a clear expansion of hypoxia in the tropics (Stramma et
15 al., 2008; Stramma et al., 2010a; Stramma et al., 2012) over recent decades, contradicting the
16 long-term predictions from models. Biases in the modeling of lateral ventilation via deep
17 equatorial jets have been suggested as possible causes for discrepancy in predictions
18 compared to observations (Stramma et al., 2010b; Getzlaff and Dietze, 2013), which could be
19 too dominated by changes in vertical ventilation. It is also possible that the observed OMZ
20 expansion in the tropics is mostly the result of natural variability on multi-decadal timescales,
21 for example driven by changes in trade winds associated with the Pacific Decadal Oscillation
22 (Deutsch et al., 2011; Czeschel et al., 2012; Deutsch et al., 2014). **Trade winds regulate the
23 strength of the subtropical-tropical cells (eg. Luebbecke et al., 2008), which modify the
24 amount of oxygen transferred from the gyres to the eastern Pacific Ocean (Duteil et al.,
25 2014b).**

26

27 **Appendix A1: Model by model analysis of physical and biological processes** 28 **contributing to biases in the Pacific Oxygen Minimum Zones**

29 All the CMIP5 models underestimate the equatorial ventilation, contributing to the anomalous
30 merging of the northern and southern OMZs in the Pacific Ocean. Here, we describe in detail
31 additional sources of bias, such as the ventilation from the Southern and North Pacific Oceans

1 and the parameterization of the remineralization profiles, which differ from model to model.
2 The following results are based on Tables A1, A2, and A3 and references therein.

3

4 **GFDL-ESM2M and GFDL-ESM2G:**

5 *Biases:*

6 Both GFDL-ESM2 models display a large tropical OMZ, overestimate the southward
7 extension of the southern OMZ, and underestimate the northward extension of the northern
8 OMZ, which results in too much hemispheric symmetry in OMZs (Fig. 1). Both models
9 overestimate the vertical depth of the OMZ (Fig. 1), despite large oxygen concentrations in
10 the deep Pacific for GFDL-ESM2G (Fig. 2).

11 *Mechanisms:*

12 Both GFDL-ESM2 models are biased towards low Southern Ocean intermediate ventilation
13 and high North Pacific ventilation (NPIW), resulting in too much hemispheric symmetry in
14 OMZs. The version ESM2M captures best the tropics, southern hemisphere, and deep Pacific
15 oxygen, while ESM2G captures best the NPIW ventilation and consequently the northern
16 OMZ. The excess in deep oxygen concentration in GFDL-ESM2G is related to large AABW
17 formation rates.

18 Both GFDL models overestimate the extension and depth of OMZ, possibly due to equatorial
19 under-ventilation that leads to nutrient trapping, and worsened by an excess of denitrification
20 (also suggested by Dunne et al., 2012) and by the use of an exponential remineralization curve
21 (Fig. 6). The OMZ shape is almost constant at different depths contrary to observations,
22 suggesting that the OMZ is indeed maintained by a vertical mechanism as it would be too
23 much POC flux and remineralization at depth. The denitrification length is considerably high
24 in GFDL-ESM2 (1500m), displacing POC remineralization and the OMZ deeper in GFDL-
25 ESM2 compared to other models. Instantaneous remineralization of POC at the bottom floor
26 (without burial of POC to the sediments) might also contribute to a too deep OMZ.

27

28 **CESM1-BGC:**

29 *Biases:*

1 CESM1-BGC represents well the overall patterns in oxygen, but overestimates the spatial
2 extent of OMZ in the equatorial Pacific (Fig. 1). CESM1-BGC displays extended negative
3 oxygen bias over most of the ocean (Moore et al., 2013). However, the NH OMZ matches the
4 depth and patterns of the observed OMZ better than most CMIP5 models (Section 3.1.4).

5 *Mechanisms:*

6 A poor equatorial ventilation system, combined with underestimated mid-depth ventilation
7 from the Southern Ocean and North Pacific results in larger-than-observed OMZ.

8 The exponential curve used to represent soft POC is a potential source of bias that could be
9 improved by applying a power law instead (Moore et al., 2013). Even though the
10 remineralization curve is exponential and similar to the models that develop a deep OMZ
11 (compare GFDL-ESM2 and CESM1-BGC remineralization curves in Fig. 6), CESM1-BGC
12 does not develop such strong denitrification or deep OMZ. The denitrification rate is higher
13 than in the other models with exponential profile (denitrification length equal to 260m instead
14 of 1500m in GFDL-ESM2), alleviating the POC displacement to deeper depths. Additionally,
15 the consumption of nitrate in denitrification is corrected to avoid a complete nitrate depletions
16 (Lindsay et al. 2014) possibly correcting for deep OMZ.

17

18 **IPSL-CM5A-MR (LR):**

19 *Biases:*

20 This model forms a large OMZ in the deep North Pacific and shows low oxygen
21 concentrations in the entire deep Pacific. However, the tropical mid-depth OMZ barely
22 develops (mid-depth oxygen is too high compared to observations).

23 *Mechanisms:*

24 The relatively low exponent in the power law remineralization curve (Fig. 6 and Table 3)
25 creates an extended deep OMZ (as also suggested by Dufresne et al., 2013) because it
26 transfers too much POC to depth shifting the OMZ to deeper depths and resulting in positive
27 oxygen anomalies in the upper layers. The underestimate of the OMZ volumes (high levels of
28 oxygen compared to observations) in the tropics and SH is also related to the fact that
29 nutrients (and hence production) are underestimated there (Fig. 2, 3) probably due to weak

1 EUC (Fig. 4). At the sea floor, all the remaining POC is buried into the sediments, a
2 mechanism which prevents further hypoxia in the bottom layers.

3

4 **MPI-ESM-MR (LR):**

5 *Biases:*

6 The tropical OMZs are too deep (as previously noted by Ilyina et al., 2013), too large, and
7 expand too far poleward in both hemispheres. However, the oxygen concentration is
8 overestimated in the deep Southern Ocean.

9 *Mechanisms:*

10 Intermediate water masses are well represented in this model. However, AABW formation is
11 **underestimated**, which **might explain** the large oxygen bias **in the deep low-latitudes and NH**.
12 Fig. 4 shows the large bias in equatorial ventilation in the low-resolution version of the model
13 (MPI-ESM-LR), which is much improved in the high-resolution version (MPI-ESM-MR).
14 However, both resolution model versions show similar biases in oxygen distribution and a
15 too-deep OMZ, suggesting that the deep OMZ is mostly due to **extra-equatorial ventilation** or
16 biological bias.

17 The modeled deep OMZ **might result** from an exponential remineralization curve with a low
18 exponent (exaggerated with low denitrification rates and complete depletion of nitrate)
19 combined with an overestimate of the POC flux from the euphotic layer (Fig. 5). The OMZ
20 forms at a shallower depth than in other models and observations due to large POC flux in the
21 euphotic layer.

22

23 **NorESM1-ME:**

24 *Biases:*

25 The oxygen in this model is too high in the entire deep Pacific and in the NH intermediate
26 depths. However, the model develops large and deep OMZs in the tropical mid-depths (Fig. 1,
27 2).

28 *Mechanisms:*

1 The level of oxygen is too high everywhere surrounding the OMZs due to excessive deep-
2 water formation that expands to the NH, and likely also enhanced by excessive NPIW mixing.

3 The OMZ is similarly deep in NorESM1-ME and MPI-ESM models. Both model groups
4 share the same biogeochemical model HAMOCC (and very similar parameters) but differ on
5 the physics, suggesting that the remineralization curve is the cause for the deep OMZ
6 extension. An exponential curve for remineralization profile transfers too much POC to depth
7 creating a deep OMZ in the Nor-ESM1 model (similar to GFDL-ESM2 and MPI-ESM
8 models). The POC flux at 100m is too large as shown in Fig. 5, contributing to the deep OMZ.

9

10 **HadGEM2-ES (CC):**

11 *Biases:*

12 These two models form a large and deep southern OMZ that expands towards the tropics.
13 However, no northern OMZ is formed resulting in a positive oxygen anomaly compared to
14 observations.

15 *Mechanisms:*

16 According to Williams et al. (2014), the globally prevalent positive oxygen bias in
17 HadGEM2-ES between 100 and 1000m at low northern latitudes can be attributed to
18 underestimation of primary productivity at mid-to-high latitudes (and subsequent low
19 consumption in the subsurface). We think that a strong NPIW also contributes to elevated
20 oxygen advection and to the removal of the northern OMZ. In the southern Pacific Ocean,
21 there is generally good agreement between observed and simulated PP and oxygen fields
22 (Williams et al., 2014), although the OMZ is too large there, possibly due to the low exponent
23 assumed in the power law remineralization curve.

24

25 **MRI-ESM1-ME:**

26 *Biases:*

27 This model shows larger-than-observed southern OMZ, and smaller-than-observed northern
28 OMZ. Additionally, oxygen concentration is overestimated at depth.

29 *Mechanisms:*

1 The amount of nitrate available in the eastern tropics and southern low-latitudes (Fig. 3) is
 2 anomalously high, causing the POC flux to be high in these zones (Fig. 5). The EUC is
 3 weaker than observed so it should not be the cause for high levels of nitrate. In this case, high
 4 levels of nitrate could be explained by trapping on the eastern side due to anomalously
 5 shallow remineralization (resulting in remineralized new nitrate). In order to match observed
 6 oxygen, a high exponent is prescribed for the exponential remineralization curve (Fig. 5). In
 7 the NH, both nitrate and POC flux are low compared to observations, hence the high exponent
 8 in the remineralization curve does not allow the NH OMZ to extend as northward as seen in
 9 observations. Moreover, the large NPIW ventilation contributes to the removal of the northern
 10 OMZ.

11

12 **Appendix A2: Tables**

13

14 **Table A1:** Summarized information across CMIP5 models. The table includes: spatial
 15 resolution in the ocean, ocean module, ecology subroutine, phytoplankton types, references,
 16 and weight applied in the multimodel averages (see Methods). **The major differences between**
 17 **HadGEM2-ES and -CC are the inclusion of an interactive tropospheric chemistry component**
 18 **in -ES, and different vertical atmospheric resolution in -ES (L30) and -CC (L60). The only**
 19 **difference between IPSL-CM5A-LR and -MR is the atmospheric horizontal resolution, 1.9° x**
 20 **3.75° for -LR (low res.) and 1.25° x 2.5° for -MR (medium res.).**

21

22

23

<i>Model</i>	<i>Resolution (depth levels, long/lat)</i>	<i>Ocean module</i>	<i>References physics</i>	<i>Ecology module</i>	<i>References biogeochemistry</i>	<i>Weight assigned in multi model statistics</i>
CESM1-BGC	60, 1.125/0.27– 0.53	CCSM4	Gent et al. (2011), Danabasoglu et al. (2012), Weijer et al. (2011)	MET	Moore et al. (2004), Moore et al. (2006), Moore et al. (2013), Moore and Doney (2007) Lindsay et al. (2014)	1
GFDL-ESM2G	63,	GOLD	Dunne et al. (2012)	TOPAZ2	Dunne et al. (2013)	1

	1/0.3-1					
GFDL-ESM2M	50, 1/0.3-1	MOM4p1	Dunne et al. (2012)	TOPAZ2	Dunne et al. (2013)	1
HadGEM2-ES (CC)	40, 1/0.3-1	HadGEM2	Collins et al. (2011), Jones et al. (2011), Martin et al. (2011)	Diat-HadOCC (NPZD)	Palmer and Totterdell (2001)	0.5 (0.5)
IPSL-CM5A-MR (LR)	31, 2/0.5-2	NEMOv3.2	Dufresne et al. (2013)	PISCES (from HAMOCC5)	Aumont and Bopp (2006), Séférian et al. (2013)	0.5 (0.5)
MPI-ESM-MR (LR)	40, 0.4/0.4 (1.5/1.5)	MPIOM	Jungclaus et al. (2013), Giorgetta et al. (2013)	HAMOCC5.2 (NPZD)	Ilyina et al. (2013)	0.5 (0.5)
NorESM1-ME	53, 1/1.25	based on CCSM4 & MICOM	Bentsen et al. (2013), Iversen et al. (2013), Tjiputra et al. (2013)	HAMOCC5.1 (NPZD)	Assmann et al. (2010)	1
MRI-ESM1	51 1/0.5	OGCM	Yukimoto et al. (2011)	NPZD	Yukimoto et al. (2011)	1

1

2

3 **Table A2:** Description of ventilation sources across CMIP5 models, including North Pacific
4 ventilation via NPIW, deep ventilation via AMOC and AABW, intermediate-depth South
5 Pacific ventilation via AAIW and SAMW, and equatorial ventilation. The diapycnal mixing
6 coefficient Aredi (collected from references in Table 1) is shown in parenthesis in the first
7 column. **The AABW strength is calculated as the maximum value of the lower cell in the**
8 **Indo-Pacific meridional streamfunction at 30°S. Fig. S9 shows the streamfunction across**
9 **CMIP5 models.** *Italic entries show contributions from the present research; regular font shows*
10 literature compilation.

11

Model (Aredi)	<i>North Pacific Ventilation</i>	<i>Deep Ocean Ventilation</i>	<i>South Pacific intermediate ventilation</i>	<i>Equatorial ventilation</i>
--------------------------------	----------------------------------	-------------------------------	---	-------------------------------

<p>CESMI-BGC (800 m/s²)</p>	<p>NPIW formation in the North Pacific is weaker than observed (Moore et al., 2013)</p>	<p>AABW transport is consistent with observations but on the weak side (Danabasoglu et al., 2012). <i>AABW_30S=5.2 Sv</i> <i>This might add to NH OMZ being too large resulting from low deep ventilation to the deep North Pacific.</i></p>	<p>Intermediate-depths AAIW and SAMW water masses are found more equatorward and weaker than observations, probably related to the underestimation of MLD near the formation region (Danabasoglu et al., 2012) <i>The Southern Hemisphere OMZ is then too large.</i></p>	<p>The sub-surface ventilation via isopycnal mixing at low-latitudes is weak, which contributes to negative biases in oxygen concentration (Moore et al., 2013). However, this version shows improvements in subsurface equatorial jets thanks to improved wind stress (usually underrepresented in low-resolution simulations). Still, the modeled wind and precipitation forcing is more N-S symmetric than the observed one. The depth and strength of EUC are well represented (Danabasoglu et al., 2012).</p>
<p>GFDL-ESM2G (M) (600 m/s²)</p>	<p>The North Pacific is overly ventilated by NPIW in ESM2M. ESM2G represents the lack of oxygen ventilation in the North Pacific better than ESM2M though still at the high end compared to observations. (Dunne et al., 2013)</p>	<p>ESM2G is overly ventilated south of 60°S, such that bottom waters in ESM2G propagate further northward than in ESM2M, resulting in younger deep waters in ESM2G than in ESM2M (Dunne et al., 2013). <i>AABW_30S=18.8 (14.2) Sv</i> <i>Larger AABW ventilation in ESM2G leads to higher levels of oxygen in the deep North Pacific.</i></p>	<p>ESM2M reproduces the observed areas of SAMW in the Southern Ocean between 40°S and 50°S while ESM2G underestimates the production of these waters. ESM2G exacerbates the ESM2M oxygen bias in the tropical and southern subtropical oceans and Southern Ocean north of 60°S (Dunne et al., 2013).</p>	<p>ESM2M lacks ventilation in the eastern equatorial Pacific, and ESM2G exacerbates this oxygen bias even more. ESM2M represents better the tropical west Pacific than ESM2G (Dunne et al., 2013), which leads to a better representation of the OMZ (<i>less expanded to the west</i>).</p>
<p>HadGEM2-ES (CC) (500 m/s²)</p>	<p><i>We suggest that an overestimation of the extension of NPIW ventilation contributes to the removal of the northern OMZ.</i></p>	<p>HadGEM2-ES has well-developed upper and lower circulatory cells which are analogous to the (upper) North Atlantic Deep Water (NADW) and (lower) Antarctic AABW systems observed (Williams et al., 2014). The AMOC is only slightly weaker than observed (Martin et al., 2011). <i>AABW_30S=12.3 (13.4) Sv</i></p>	<p>HadGEM2-ES subducts intermediate waters in regions of the water column that are clearly too stratified (Sallee et al., 2013b). <i>The SH OMZ is then too large because of poor intermediate ventilation.</i></p>	<p><i>EUC too weak towards the East (Fig. 4), resulting in underestimated transport of nitrate, low primary production and low POC flux.</i></p>
<p>IPSL-CM5A-MR (LR) (1000 m/s²)</p>	<p><i>We suggest that NPIW expands too deep, which contributes to the overestimation of oxygen in the northern OMZ regions.</i></p>	<p><i>AABW_30S=15.3 (13.5) Sv</i> <i>The strength of AABW is normal among CMIP5 models.</i></p>	<p><i>No reported bias in AAIW or SAMW.</i></p>	<p>The model tends to underestimate the high surface nutrient concentrations that are associated with the strong Equatorial Pacific upwelling on the eastern side (Dufresne et al., 2013). <i>This is due to deficient eastward EUC velocity (Fig. 4). As a consequence, local PP is underestimated, and so it is the OMZ extension.</i></p>
<p>MPI-ESM-MR (LR) (1000 m/s²)</p>	<p><i>NPIW well represented.</i></p>	<p><i>AABW_30S = 7.9 (6.5) Sv</i> <i>Our calculated AABW in Pacific is among the lowest across CMIP5 models, which could contribute to a negative oxygen bias in the</i></p>	<p>This model represents fairly well mid-depth AAIW and SAMW (Fig. 4, Junclaus et al., 2013).</p>	<p>Introducing an "eddy-permitting" grid configuration (MPI-ESM-MR, 0.4° precision) in the ocean leads to improvements in the representation of the Equatorial current systems (Junclaus et al., 2013). In particular, the position</p>

		<i>deep tropics and NH.</i>		of the maximum and the tilt of the core of the equatorial undercurrent (EUC) with depth are well captured in the MPI-ESM-MR model.
NorESM1-ME	<i>NPIW is too deep and poleward compared to observations, which contributes to the removal of the northern OMZ.</i>	The AMOC strength is in the upper range among models contributing to phase 3 of the Climate Model Intercomparison Project (CMIP3) and well above observations. It is not clear what causes the vigorous AMOC intensity (Bentsen et al., 2013). <i>AABW_30S = 21.9 Sv</i> <i>This results into anomalously large oxygen concentration at depth and too small NH OMZ.</i>	The model realistically simulates the structure of AAIW and SAMW from the Southern Ocean (Tjiputra et al., 2013). <i>However, these waters seem to carry too low oxygen concentrations (Fig. 2)</i>	<i>EUC is well captured in this model (Fig. 4).</i>
MRI-ESM1	<i>NPIW is too deep and poleward compared to observations, which contributes to the removal of the northern OMZ.</i>	<i>AABW_30S = 9.9 Sv</i> <i>The strength of AABW is normal among CMIP5 models.</i>	<i>We hypothesize that AAIW waters are deficient in this model (based on Fig. 2).</i>	<i>EUC is too weak in this model (Fig. 4).</i>

1

2 **Table A3:** Description of biological parameters that might affect OMZ extension, including
3 POC flux profile, denitrification, nitrogen fixation, and sediment burial across CMIP5 models,
4 summarized from references in Table A1 and our analysis (see also Supp Fig. S1). Most
5 CMIP5 biogeochemical models use a constant rate of remineralization r combined with a
6 constant sinking speed of POC or a sinking speed increasing with depth. In the case of
7 linearly increasing sinking speed $w(z)=w_0+a \cdot z$ and the POC flux profile (F_{POC}) follows a
8 classical Martin power-law curve $F_{POC}(z)=F_{POC}(z_0)(z/z_0)^{-b}$ with b equal to r/a . In the constant
9 sinking speed case the POC flux profile follows an exponential curve $F_{POC}(z)=F_{POC}(z_0)\exp(-$
10 $b \cdot z)$ with b equal to r/w (Kriest and Oschlies 2008). Some models with exponential POC
11 profile give the exponent in terms of remineralization length λ , equivalent to $1/b$.

12

Model	POC flux	Denitrification	Nitrogen fixation	Sediment remineralization
--------------	-----------------	------------------------	--------------------------	----------------------------------

<p style="text-align: center;">CESM1-BGC</p>	<p>Ballast model (Armstrong et al., 2002) with two sinking classes: a) a soft POC that remineralizes at a fixed length scale ($l=130\text{m}$) with temperature dependence, and constitutes $>90\%$ of the POC leaving the euphotic layer. b) a class strongly associated with mineral ballast types (including lithogenic particles, biogenic silica, and calcium carbonate), with deeper remineralization lengths.</p> <p>$F_{\text{POC}}(z)/F_{\text{POC}}(z=z_0)=\exp(-(z-z_0)T_f^{\text{POC}}/l)$</p> <p><i>Curve dominated by soft POC at mid-depths, and by ballast POC at depth (sum of exponentials with different exponents).</i></p> <p><i>POC flux at 100m is more smoothly distributed than in the other models (Sup. Fig. S1), and it is large everywhere in the tropics, which could explain partially why OMZ expands so much to the west.</i></p>	<p>Switch to denitrification at $O_2 < 4 \text{ mmol/m}^3$ ($l_{\text{denit}}=260\text{m}$), based on Van Mooy et al. (2002), but corrected to avoid artificially deep OMZ via nitrate run out, by multiplying the fixed N removal rate times the simulated nitrate concentration divided by a factor of 110 (Moore et al. 2013).</p> <p><i>As the removal of nitrate necessary to degrade POC is artificially reduced, there is no nitrate run out, such that POC remineralization can continue. Avoiding complete run out of nitrate should partially fix OMZ.</i></p>	<p>Diazotrophs fix dissolved N_2 (with iron limitation).</p> <p>In the Pacific, simulated export is driven by upwelling with less influence by N fixation. N fixation had a modest impact on the organic flux sinking into the OMZs (Moore et al. 2007)</p>	<p>All the remaining POC is remineralized instantaneously when reaching the sea floor.</p>
<p style="text-align: center;">TOPAZ2 (GFDL-ESM2G, GFDL-ESM2M)</p>	<p>Ballast model (Armstrong et al. 2002) with two sinking classes: a) a soft (unprotected) POC that remineralizes at a fixed length scale (rate $r=0.016/\text{d}$, sinking speed $w=3\text{m/d}$, $l=187.5\text{m}$) b) a protected class strongly associated with mineral ballast types (biogenic silica, and calcium carbonate), with deeper remineralization scales. Part of this class is converted to soft POC at each depth.</p> <p>$F_{\text{POC}}(z)/F_{\text{POC}}(z=z_0)=\exp(-(z-z_0)t/w)$</p> <p><i>Curve dominated by soft POC at mid-depths, and by ballast at depth (sum of exponentials with different exponents).</i></p> <p><i>POC flux at 100m is high in the tropics and high latitudes (Sup. Fig. S1), similar to observations. As a result of its more vigorous thermocline ventilation, ESM2M has higher total primary production and POC flux than ESM2G in most ocean areas.</i></p>	<p>Switch to denitrification at $O_2 < 5 \text{ mmol/m}^3$ (with minimum nitrate condition $\text{NO}_3 > 0.1 \text{ mmol/m}^3$)</p> <p>Rate $r_{\text{denit}}=0.002/\text{d}$ (8 times less than oxic remineralization, $l_{\text{denit}}=1500\text{m}$)</p> <p>In the absence of both NO_3 and O_2, a respiration deficit is accumulated as negative O_2 (Dunne et al. 2013).</p>	<p>Diazotrophs fix dissolved N_2 (with iron limitation).</p>	<p>All the remaining POC is remineralized on the bottom floor instantaneously (J.Dunne personal communication).</p>

<p>HadGEM2-ES (CC)</p>	<p>POC flux in the form of slow-sinking detritus (10m/d) with specific remineralization rate varying inversely with depth (Martin-style power law but capped).</p> $F_{POC}(z)/F_{POC}(z=z_0)=(z/z_0)^{-b}$ <p><i>Consistent with a power law curve (below 100m) with exponent b equal to 0.7 (Fig. 6).</i></p> <p><i>POC flux at 100m follows the expected patterns (Sup. Fig. S1). However, low POC in the eastern tropical Pacific contributes to positive biases in oxygen in the OMZ regions.</i></p>	<p>No denitrification</p>	<p>No nitrogen fixation</p>	<p>All detrital material reaching the sea-floor is instantly remineralized. New-remineralized material is spread evenly over lowest three layers. Sinking diatoms that hit the sea floor die instantly, becoming detritus.</p>
<p>PISCES (IPSL-CM5A)</p>	<p>Two types of POC, POCs (small) and POCb (big). Only POCb changes sinking speed with depth.</p> $F_{POC}(z)/F_{POC}(z=z_0)=(z/z_0)^{-b}$ <p><i>The total POC remineralization curve is the sum of two power laws, as big and small POC have different exponents.</i></p> <p><i>Change in POC approximately consistent with a power law curve with exponent b varying from 0.75 at intermediate depths to 0.5 at depth (obtained from Fig.6).</i></p>	<p>Remineralization changes linearly from oxic to anoxic (denitrification) at oxygen levels between 6 mmol/m³ (all oxic) and 1 mmol/m³ (all denitrification). The rate of denitrification is the same than the rate of oxic remineralization.</p>	<p>Nitrogen fixation is parametrized in a crude way:</p> <ul style="list-style-type: none"> - Restricted to warm waters above 20°C - Restricted to area with insufficient nitrogen fixation - It requires iron - Restricted to the sea surface - To ensure N conservation in the ocean, annual total nitrogen fixation should balance denitrification. 	<p>In PISCES sinking organic matter is permanently buried below the sea floor, thereby preventing the accumulation of detritus and slow remineralization at the bottom.</p>
<p>HAMOC (MPI-ESM, NorESM1-ME)</p>	<p>POC in the form of detritus (remin. rate r=0.025/d, sinking speed of detritus w=5 m/d, l=200 m)</p> $F_{POC}(z)/F_{POC}(z=z_0)=\exp(-(z-z_0) r/w)$ <p><i>POC flux at 100m is too high in the eastern side of the tropical Pacific for both MPI-ESM and NorESM1-ME (Sup. Fig. S1). This contributes to teh formation of a large OMZ. In MPI-ESM, POC flux is also high in the western tropics.</i></p>	<p>At low oxygen levels (O₂ < 0.5 mmol/m³), switch to denitrification and sulfur reduction.</p> <p>Denitrification rate 0.005 /d (5 times less than oxic remineralization, l_{denit}=1000 m)</p>	<p>In nitrate-limited oligotrophic regions, the model assumes nitrogen fixation by cyanobacteria, which is parameterized as the relaxation of the nitrate concentration at surface layer to the available phosphate concentration, through Redfield ratio. In a stationary ocean, denitrification and nitrogen fixation are balanced.</p>	<p>The sediment model used is based on Heinze et al. (1999). Within the sediment, remineralization of organic material is described as in the water column: aerobic remineralization occurs as long as oxygen is available in pore water, taking into account that part of the sediments becomes unavailable at each time step.</p>
<p>MRI-ESM1</p>	<p>POC in the form of detritus (remin. rate r=0.048/day, sinking speed of detritus w=2m/day, l=41.66 m)</p> $F_{POC}(z)/F_{POC}(z=z_0)=\exp(-(z-z_0) r/w)$ <p><i>POC flux at 100m is too high in the tropics and Eastern Pacific (Fig. S1), possibly due to high subsurface recycling of organic matter associated with overestimated nitrate.</i></p>	<p>No denitrification</p>	<p>No nitrogen fixation</p>	

1

2 Acknowledgements

1 A. C. and I. M. acknowledge support by NASA ROSES grant NNX13AC92G and by a University of
2 Pennsylvania research foundation grant. R. B. was sponsored by NOAA Grant NOAA-
3 NA10OAR4310092. We would like to thank J. Dunne, S. Henson, and D. Siegel for sharing their data
4 results.

5

6 **References**

- 7 Armstrong, R. A., Lee, C., Hedges, J. I., Honjo, S., and Wakeham, S. G.: A new, mechanistic model for
8 organic carbon fluxes in the ocean based on the quantitative association of POC with ballast minerals,
9 *Deep-Sea Research Part II-Topical Studies in Oceanography*, 49, 219-236, 2002.
- 10 Ascani, F., Firing, E., Dutrieux, P., McCreary, J. P., and Ishida, A.: Deep Equatorial Ocean Circulation
11 Induced by a Forced-Dissipated Yanai Beam, *Journal of Physical Oceanography*, 40, 1118-1142,
12 10.1175/2010jpo4356.1, 2010.
- 13 Assmann, K. M., Bentsen, M., Segschneider, J., and Heinze, C.: An isopycnic ocean carbon cycle model,
14 *Geoscientific Model Development*, 3, 143-167, 2010.
- 15 Aumont, O., Orr, J. C., Monfray, P., Madec, G., and Maier-Reimer, E.: Nutrient trapping in the equatorial
16 Pacific: The ocean circulation solution, *Global Biogeochemical Cycles*, 13, 351-369, 1999.
- 17 Aumont, O., and Bopp, L.: Globalizing results from ocean in situ iron fertilization studies, *Global*
18 *Biogeochemical Cycles*, 20, 15, 10.1029/2005gb002591, 2006.
- 19 Bentsen, M., Bethke, I., Debernard, J. B., Iversen, T., Kirkevåg, A., Seland, O., Drange, H., Roelandt, C.,
20 Seierstad, I. A., Hoose, C., and Kristjansson, J. E.: The Norwegian Earth System Model, NorESM1-M
21 - Part 1: Description and basic evaluation of the physical climate, *Geoscientific Model Development*,
22 6, 687-720, 10.5194/gmd-6-687-2013, 2013.
- 23 **Bernardello, R., Marinov, I., Palter, J. B., Sarmiento, J. L., Galbraith, E. D., Slater, R. D.: Response of**
24 **the ocean natural carbon storage to projected twenty-first-century climate change, *Journal of***
25 ***Climate*, 27 (5), 2033-2053, 10.1175/JCLI-D-13-00343.1, 2014.**
- 26 Bianchi, D., Dunne, J. P., Sarmiento, J. L., and Galbraith, E. D.: Data-based estimates of suboxia,
27 denitrification, and N₂O production in the ocean and their sensitivities to dissolved O₂, *Global*
28 *Biogeochemical Cycles*, 26, 13, 10.1029/2011gb004209, 2012.
- 29 Bograd, S. J., Castro, C. G., Di Lorenzo, E., Palacios, D. M., Bailey, H., Gilly, W., and Chavez, F. P.: Oxygen
30 declines and the shoaling of the hypoxic boundary in the California Current, *Geophysical Research*
31 *Letters*, 35, 10.1029/2008gl034185, 2008.
- 32 Bopp, L., Le Quere, C., Heimann, M., Manning, A. C., and Monfray, P.: Climate-induced oceanic oxygen

1 fluxes: Implications for the contemporary carbon budget, *Global Biogeochemical Cycles*, 16,
2 10.1029/2001gb001445, 2002.

3 Bopp, L., Resplandy, L., Orr, J. C., Doney, S. C., Dunne, J. P., Gehlen, M., Halloran, P., Heinze, C., Ilyina, T.,
4 Seferian, R., Tjiputra, J., and Vichi, M.: Multiple stressors of ocean ecosystems in the 21st century:
5 projections with CMIP5 models, *Biogeosciences*, 10, 6225-6245, 10.5194/bg-10-6225-2013, 2013.

6 Brandt, P., Hormann, V., Bourles, B., Fischer, J., Schott, F. A., Stramma, L., and Dengler, M.: Oxygen tongues
7 and zonal currents in the equatorial Atlantic, *Journal of Geophysical Research-Oceans*, 113,
8 10.1029/2007jc004435, 2008.

9 Cabré, A., Marinov, I., and Leung, S.: Consistent global responses of marine ecosystems to future
10 climate change across the IPCC AR5 Earth System Models, *Climate Dynamics*, 1-28,
11 10.1007/s00382-014-2374-3, 2014

12 Chan, F., Barth, J. A., Lubchenco, J., Kirincich, A., Weeks, H., Peterson, W. T., and Menge, B. A.: Emergence
13 of anoxia in the California current large marine ecosystem, *Science*, 319, 920-920,
14 10.1126/science.1149016, 2008.

15 Cocco, V., Joos, F., Steinacher, M., Frolicher, T. L., Bopp, L., Dunne, J., Gehlen, M., Heinze, C., Orr, J.,
16 Oeschlies, A., Schneider, B., Segsneider, J., and Tjiputra, J.: Oxygen and indicators of stress for
17 marine life in multi-model global warming projections, *Biogeosciences*, 10, 1849-1868, 10.5194/bg-
18 10-1849-2013, 2013.

19 Collins, W. J., Bellouin, N., Doutriaux-Boucher, M., Gedney, N., Halloran, P., Hinton, T., Hughes, J., Jones,
20 C. D., Joshi, M., Liddicoat, S., Martin, G., O'Connor, F., Rae, J., Senior, C., Sitch, S., Totterdell, I.,
21 Wiltshire, A., and Woodward, S.: Development and evaluation of an Earth-System model-HadGEM2,
22 *Geoscientific Model Development*, 4, 1051-1075, 10.5194/gmd-4-1051-2011, 2011.

23 Czeschel, R., Stramma, L., and Johnson, G. C.: Oxygen decreases and variability in the eastern equatorial
24 Pacific, *Journal of Geophysical Research-Oceans*, 117, 10.1029/2012jc008043, 2012.

25 Danabasoglu, G., Bates, S. C., Briegleb, B. P., Jayne, S. R., Jochum, M., Large, W. G., Peacock, S., and
26 Yeager, S. G.: The CCSM4 Ocean Component, *Journal of Climate*, 25, 1361-1389, 10.1175/jcli-d-11-
27 00091.1, 2012.

28 Deutsch, C., Brix, H., Ito, T., Frenzel, H., and Thompson, L.: Climate-Forced Variability of Ocean Hypoxia,
29 *Science*, 333, 336-339, 10.1126/science.1202422, 2011.

30 Deutsch, C., Berelson, W., Thunell, R., Weber, T., Tems, C., McManus, J., Crusius, J., Ito, T., Baumgartner,
31 T., Ferreira, V., Mey, J., and van Geen, A.: OCEANOGRAPHY Centennial changes in North Pacific
32 anoxia linked to tropical trade winds, *Science*, 345, 665-668, 10.1126/science.1252332, 2014.

- 1 Dietze, H., and Loeptien, U.: Revisiting "nutrient trapping" in global coupled biogeochemical ocean
2 circulation models, *Global Biogeochemical Cycles*, 27, 265-284, 10.1002/gbc.20029, 2013.
- 3 Downes, S. M., Bindoff, N. L., and Rintoul, S. R.: Changes in the Subduction of Southern Ocean Water
4 Masses at the End of the Twenty-First Century in Eight IPCC Models, *Journal of Climate*, 23, 6526-
5 6541, 10.1175/2010jcli3620.1, 2010.
- 6 Dufresne, J. L., Foujols, M. A., Denvil, S., Caubel, A., Marti, O., Aumont, O., Balkanski, Y., Bekki, S.,
7 Bellenger, H., Benshila, R., Bony, S., Bopp, L., Braconnot, P., Brockmann, P., Cadule, P., Cheruy, F.,
8 Codron, F., Cozic, A., Cugnet, D., de Noblet, N., Duvel, J. P., Ethe, C., Fairhead, L., Fichefet, T.,
9 Flavoni, S., Friedlingstein, P., Grandpeix, J. Y., Guez, L., Guilyardi, E., Hauglustaine, D., Hourdin, F.,
10 Idelkadi, A., Ghattas, J., Joussaume, S., Kageyama, M., Krinner, G., Labetoulle, S., Lahellec, A.,
11 Lefebvre, M. P., Lefevre, F., Levy, C., Li, Z. X., Lloyd, J., Lott, F., Madec, G., Mancip, M.,
12 Marchand, M., Masson, S., Meurdesoif, Y., Mignot, J., Musat, I., Parouty, S., Polcher, J., Rio, C.,
13 Schulz, M., Swingedouw, D., Szopa, S., Talandier, C., Terray, P., Viovy, N., and Vuichard, N.:
14 Climate change projections using the IPSL-CM5 Earth System Model: from CMIP3 to CMIP5,
15 *Climate Dynamics*, 40, 2123-2165, 10.1007/s00382-012-1636-1, 2013.
- 16 Dunne, J. P., Armstrong, R. A., Gnanadesikan, A., and Sarmiento, J. L.: Empirical and mechanistic models for
17 the particle export ratio, *Global Biogeochemical Cycles*, 19, 10.1029/2004gb002390, 2005.
- 18 Dunne, J. P., John, J. G., Adcroft, A. J., Griffies, S. M., Hallberg, R. W., Shevliakova, E., Stouffer, R. J.,
19 Cooke, W., Dunne, K. A., Harrison, M. J., Krasting, J. P., Malyshev, S. L., Milly, P. C. D., Phillipps,
20 P. J., Sentman, L. T., Samuels, B. L., Spelman, M. J., Winton, M., Wittenberg, A. T., and Zadeh, N.:
21 GFDL's ESM2 Global Coupled Climate-Carbon Earth System Models. Part I: Physical Formulation
22 and Baseline Simulation Characteristics, *Journal of Climate*, 25, 6646-6665, 10.1175/jcli-d-11-
23 00560.1, 2012.
- 24 Dunne, J. P., John, J. G., Shevliakova, E., Stouffer, R. J., Krasting, J. P., Malyshev, S. L., Milly, P. C. D.,
25 Sentman, L. T., Adcroft, A. J., Cooke, W., Dunne, K. A., Griffies, S. M., Hallberg, R. W., Harrison,
26 M. J., Levy, H., Wittenberg, A. T., Phillips, P. J., and Zadeh, N.: GFDL's ESM2 Global Coupled
27 Climate-Carbon Earth System Models. Part II: Carbon System Formulation and Baseline Simulation
28 Characteristics, *Journal of Climate*, 26, 2247-2267, 10.1175/jcli-d-12-00150.1, 2013.
- 29 Duteil, O., Schwarzkopf, F. U., Boning, C. W., and Oschlies, A.: Major role of the equatorial current system in
30 setting oxygen levels in the eastern tropical Atlantic Ocean: A high- resolution model study,
31 *Geophysical Research Letters*, 41, 2033-2040, 10.1002/2013gl058888, 2014.
- 32 Duteil, O., Böning, C. W., and Oschlies, A.: Variability in subtropical-tropical cells drives oxygen
33 levels in the tropical Pacific Ocean, *Geophys. Res. Lett.*, 41, 8926–8934,
34 doi:10.1002/2014GL061774, 2014b.

- 1 Eden, C., and Dengler, M.: Stacked jets in the deep equatorial Atlantic Ocean, *Journal of Geophysical*
2 *Research-Oceans*, 113, 10.1029/2007jc004298, 2008.
- 3 Emerson, S., Watanabe, Y. W., Ono, T., and Mecking, S.: Temporal trends in apparent oxygen utilization in
4 the upper pycnocline of the North Pacific: 1980-2000, *Journal of Oceanography*, 60, 139-147,
5 10.1023/B:JOCE.0000038323.62130.a0, 2004.
- 6 Friedlingstein, P., Meinshausen, M., Arora, V. K., Jones, C. D., Anav, A., Liddicoat, S. K., and Knutti, R.:
7 Uncertainties in CMIP5 Climate Projections due to Carbon Cycle Feedbacks, *Journal of Climate*, 27,
8 511-526, 10.1175/jcli-d-12-00579.1, 2014.
- 9 Fuenzalida, R., Schneider, W., Garces-Vargas, J., Bravo, L., and Lange, C.: Vertical and horizontal extension
10 of the oxygen minimum zone in the eastern South Pacific Ocean, *Deep-Sea Research Part II-Topical*
11 *Studies in Oceanography*, 56, 1027-1038, 10.1016/j.dsr2.2008.11.001, 2009.
- 12 Garcia, H. E., and Gordon, L. I.: OXYGEN SOLUBILITY IN SEAWATER - BETTER FITTING
13 EQUATIONS, *Limnology and Oceanography*, 37, 1307-1312, 1992.
- 14 Gent, P. R., Danabasoglu, G., Donner, L. J., Holland, M. M., Hunke, E. C., Jayne, S. R., Lawrence, D. M.,
15 Neale, R. B., Rasch, P. J., Vertenstein, M., Worley, P. H., Yang, Z. L., and Zhang, M. H.: The
16 Community Climate System Model Version 4, *Journal of Climate*, 24, 4973-4991,
17 10.1175/2011jcli4083.1, 2011.
- 18 Getzlaff, J., and Dietze, H.: Effects of increased isopycnal diffusivity mimicking the unresolved equatorial
19 intermediate current system in an earth system climate model, *Geophysical Research Letters*, 40,
20 2166-2170, 10.1002/grl.50419, 2013.
- 21 Giorgetta, M. A., Jungclaus, J., Reick, C. H., Legutke, S., Bader, J., Bottinger, M., Brovkin, V., Crueger, T.,
22 Esch, M., Fieg, K., Glushak, K., Gayler, V., Haak, H., Hollweg, H. D., Ilyina, T., Kinne, S.,
23 Kornbluh, L., Matei, D., Mauritsen, T., Mikolajewicz, U., Mueller, W., Notz, D., Pithan, F., Raddatz,
24 T., Rast, S., Redler, R., Roeckner, E., Schmidt, H., Schnur, R., Segschneider, J., Six, K. D.,
25 Stockhause, M., Timmreck, C., Wegner, J., Widmann, H., Wieners, K. H., Claussen, M., Marotzke, J.,
26 and Stevens, B.: Climate and carbon cycle changes from 1850 to 2100 in MPI-ESM simulations for
27 the Coupled Model Intercomparison Project phase 5, *Journal of Advances in Modeling Earth Systems*,
28 5, 572-597, 10.1002/jame.20038, 2013.
- 29 Gnanadesikan, A., Russell, J. L., and Zeng, F.: How does ocean ventilation change under global warming?,
30 *Ocean Science*, 3, 43-53, 2007.
- 31 Gnanadesikan, A., Dunne, J. P., and John, J.: Understanding why the volume of suboxic waters does not
32 increase over centuries of global warming in an Earth System Model, *Biogeosciences*, 9, 1159-1172,
33 10.5194/bg-9-1159-2012, 2012.

- 1 Gnanadesikan, A., Bianchi, D., and Pradal, M. A.: Critical role for mesoscale eddy diffusion in supplying
2 oxygen to hypoxic ocean waters, *Geophysical Research Letters*, 40, 5194-5198, 10.1002/grl.50998,
3 2013.
- 4 Gray, J. S., Wu, R. S. S., and Or, Y. Y.: Effects of hypoxia and organic enrichment on the coastal marine
5 environment, *Marine Ecology Progress Series*, 238, 249-279, 10.3354/meps238249, 2002.
- 6 Helm, K. P., Bindoff, N. L., and Church, J. A.: Observed decreases in oxygen content of the global ocean,
7 *Geophysical Research Letters*, 38, 10.1029/2011gl049513, 2011.
- 8 Henson, S. A., Sanders, R., and Madsen, E.: Global patterns in efficiency of particulate organic carbon export
9 and transfer to the deep ocean, *Global Biogeochemical Cycles*, 26, 10.1029/2011gb004099, 2012.
- 10 Ilyina, T., Six, K. D., Segschneider, J., Maier-Reimer, E., Li, H. M., and Nunez-Riboni, I.: Global ocean
11 biogeochemistry model HAMOCC: Model architecture and performance as component of the MPI-
12 Earth system model in different CMIP5 experimental realizations, *Journal of Advances in Modeling
13 Earth Systems*, 5, 287-315, 10.1029/2012ms000178, 2013.
- 14 Ito, T., Follows, M. J., and Boyle, E. A.: Is AOU a good measure of respiration in the oceans?, *Geophysical
15 Research Letters*, 31, 10.1029/2004gl020900, 2004.
- 16 Ito, T., and Deutsch, C.: Variability of the oxygen minimum zone in the tropical North Pacific during the late
17 twentieth century, *Global Biogeochemical Cycles*, 27, 1119-1128, 10.1002/2013gb004567, 2013.
- 18 Iversen, T., Bentsen, M., Bethke, I., Debernard, J. B., Kirkevåg, A., Seland, O., Drange, H., Kristjansson, J. E.,
19 Medhaug, I., Sand, M., and Seierstad, I. A.: The Norwegian Earth System Model, NorESM1-M - Part
20 2: Climate response and scenario projections, *Geoscientific Model Development*, 6, 389-415,
21 10.5194/gmd-6-389-2013, 2013.
- 22 Johnson, G. C., Sloyan, B. M., Kessler, W. S., and McTaggart, K. E.: Direct measurements of upper ocean
23 currents and water properties across the tropical Pacific during the 1990s, *Progress in Oceanography*,
24 52, 31-61, 10.1016/s0079-6611(02)00021-6, 2002.
- 25 Jones, C. D., Hughes, J. K., Bellouin, N., Hardiman, S. C., Jones, G. S., Knight, J., Liddicoat, S., O'Connor, F.
26 M., Andres, R. J., Bell, C., Boo, K. O., Bozzo, A., Butchart, N., Cadule, P., Corbin, K. D., Doutriaux-
27 Boucher, M., Friedlingstein, P., Gornall, J., Gray, L., Halloran, P. R., Hurtt, G., Ingram, W. J.,
28 Lamarque, J. F., Law, R. M., Meinshausen, M., Osprey, S., Palin, E. J., Chini, L. P., Raddatz, T.,
29 Sanderson, M. G., Sellar, A. A., Schurer, A., Valdes, P., Wood, N., Woodward, S., Yoshioka, M., and
30 Zerroukat, M.: The HadGEM2-ES implementation of CMIP5 centennial simulations, *Geoscientific
31 Model Development*, 4, 543-570, 10.5194/gmd-4-543-2011, 2011.
- 32 Jungclaus, J. H., Fischer, N., Haak, H., Lohmann, K., Marotzke, J., Matei, D., Mikolajewicz, U., Notz, D., and
33 von Storch, J. S.: Characteristics of the ocean simulations in the Max Planck Institute Ocean Model

1 (MPIOM) the ocean component of the MPI-Earth system model, *Journal of Advances in Modeling*
2 *Earth Systems*, 5, 422-446, 10.1002/jame.20023, 2013.

3 Kaplan, A., Kushnir, Y., and Cane, M. A.: Reduced space optimal interpolation of historical marine sea level
4 pressure: 1854-1992, *Journal of Climate*, 13, 2987-3002, 10.1175/1520-
5 0442(2000)013<2987:rsioih>2.0.co;2, 2000.

6 Karstensen, J., Stramma, L., and Visbeck, M.: Oxygen minimum zones in the eastern tropical Atlantic and
7 Pacific oceans, *Progress in Oceanography*, 77, 331-350, 10.1016/j.pocean.2007.05.009, 2008.

8 Keeling, R. F., and Garcia, H. E.: The change in oceanic O₂ inventory associated with recent global warming,
9 *Proceedings of the National Academy of Sciences of the United States of America*, 99, 7848-7853,
10 10.1073/pnas.122154899, 2002.

11 Keeling, R. F., Kortzinger, A., and Gruber, N.: Ocean Deoxygenation in a Warming World, *Annual Review of*
12 *Marine Science*, 2, 199-229, 10.1146/annurev.marine.010908.163855, 2010.

13 Kriest, I., Khatiwala, S., and Oschlies, A.: Towards an assessment of simple global marine biogeochemical
14 models of different complexity, *Progress in Oceanography*, 86, 337-360,
15 10.1016/j.pocean.2010.05.002, 2010.

16 Kriest, I., Oschlies, A., and Khatiwala, S.: Sensitivity analysis of simple global marine biogeochemical
17 models, *Global Biogeochemical Cycles*, 26, 10.1029/2011gb004072, 2012.

18 Kriest, I., and Oschlies, A.: Swept under the carpet: organic matter burial decreases global ocean
19 biogeochemical model sensitivity to remineralization length scale, *Biogeosciences*, 10, 8401-8422,
20 10.5194/bg-10-8401-2013, 2013.

21 Landolfi, A., Dietze, H., Koeve, W., and Oschlies, A.: Overlooked runaway feedback in the marine
22 nitrogen cycle: the vicious cycle, *Biogeosciences*, 10, 1351-1363, 2013
23 10.5194/bg-10-1351-2013, 2013

24 Li, G., and Xie, S. P.: Tropical Biases in CMIP5 Multimodel Ensemble: The Excessive Equatorial Pacific Cold
25 Tongue and Double ITCZ Problems, *Journal of Climate*, 27, 1765-1780, 10.1175/jcli-d-13-00337.1,
26 2014.

27 Lindsay, K., Bonan, G. B., Doney, S. C., Hoffman, F. M., Lawrence, D. M., Long, M. C., Mahowald, N. M.,
28 Moore, J. K., Randerson, J. T., and Thornton, P. E.: Preindustrial-Control and Twentieth-Century
29 Carbon Cycle Experiments with the Earth System Model CESM1(BGC), *Journal of Climate*, 27,
30 8981-9005, 10.1175/JCLI-D-12-00565.1, 2014.

31 Llanillo, P. J., Karstensen, J., Pelegri, J. L., and Stramma, L.: Physical and biogeochemical forcing of oxygen
32 and nitrate changes during El Niño/El Viejo and La Niña/La Vieja upper-ocean phases in the tropical
33 eastern South Pacific along 86 degrees W, *Biogeosciences*, 10, 6339-6355, 10.5194/bg-10-6339-2013,

1 2013.

2 Lübbecke, J. F., Böning, C. W., and Biastoch, A.: Variability in the subtropical-tropical cells and its
3 effect on near-surface temperature of the equatorial Pacific: a model study, *Ocean Sci.*, 4, 73-
4 88, doi:10.5194/os-4-73-2008, 2008

5 Marsay, C. M., Sanders, R. J., Henson, S. A., Pabortsava, K., Achterberg, E. P., and Lampitt, R. S.:
6 Attenuation of sinking particulate organic carbon flux through the mesopelagic ocean,
7 Proceedings of the National Academy of Sciences of the United States of America, 112, 4,
8 10.1073/pnas.1415311112, 2014.

9 Martin, G. M., Bellouin, N., Collins, W. J., Culverwell, I. D., Halloran, P. R., Hardiman, S. C., Hinton, T. J.,
10 Jones, C. D., McDonald, R. E., McLaren, A. J., O'Connor, F. M., Roberts, M. J., Rodriguez, J. M.,
11 Woodward, S., Best, M. J., Brooks, M. E., Brown, A. R., Butchart, N., Dearden, C., Derbyshire, S. H.,
12 Dharssi, I., Doutriaux-Boucher, M., Edwards, J. M., Falloon, P. D., Gedney, N., Gray, L. J., Hewitt, H.
13 T., Hobson, M., Huddleston, M. R., Hughes, J., Ineson, S., Ingram, W. J., James, P. M., Johns, T. C.,
14 Johnson, C. E., Jones, A., Jones, C. P., Joshi, M. M., Keen, A. B., Liddicoat, S., Lock, A. P., Maidens,
15 A. V., Manners, J. C., Milton, S. F., Rae, J. G. L., Ridley, J. K., Sellar, A., Senior, C. A., Totterdell, I.
16 J., Verhoef, A., Vidale, P. L., Wiltshire, A., and Had, G. E. M. D. T.: The HadGEM2 family of Met
17 Office Unified Model climate configurations, *Geoscientific Model Development*, 4, 723-757,
18 10.5194/gmd-4-723-2011, 2011.

19 Martin, J. H., Knauer, G. A., Karl, D. M., and Broenkow, W. W.: VERTEX - CARBON CYCLING IN THE
20 NORTHEAST PACIFIC, *Deep-Sea Research Part a-Oceanographic Research Papers*, 34, 267-285,
21 10.1016/0198-0149(87)90086-0, 1987.

22 Matear, R. J., and Hirst, A. C.: Long-term changes in dissolved oxygen concentrations in the ocean caused by
23 protracted global warming, *Global Biogeochemical Cycles*, 17, 10.1029/2002gb001997, 2003.

24 McClatchie, S., Goericke, R., Cosgrove, R., Auad, G., and Vetter, R.: Oxygen in the Southern California
25 Bight: Multidecadal trends and implications for demersal fisheries, *Geophysical Research Letters*, 37,
26 10.1029/2010gl044497, 2010.

27 Meijers, A. J. S.: The Southern Ocean in the Coupled Model Intercomparison Project phase 5, *Philosophical*
28 *Transactions of the Royal Society a-Mathematical Physical and Engineering Sciences*, 372,
29 10.1098/rsta.2013.0296, 2014.

30 Meinshausen, M., Smith, S. J., Calvin, K., Daniel, J. S., Kainuma, M. L. T., Lamarque, J. F., Matsumoto, K.,
31 Montzka, S. A., Raper, S. C. B., Riahi, K., Thomson, A., Velders, G. J. M., and van Vuuren, D. P. P.:
32 The RCP greenhouse gas concentrations and their extensions from 1765 to 2300, *Climatic Change*,
33 109, 213-241, 10.1007/s10584-011-0156-z, 2011.

- 1 Montes, I., Dewitte, B., Gutknecht, E., Paulmier, A., Dadou, I., Oeschies, A., and Garçon, V.: High-resolution
2 modeling of the Eastern Tropical Pacific oxygen minimum zone: Sensitivity to the tropical oceanic
3 circulation, *Journal of Geophysical Research-Oceans*, 119, 5515-5532, 10.1002/2014jc009858, 2014.
- 4 Moore, J. K., Doney, S. C., and Lindsay, K.: Upper ocean ecosystem dynamics and iron cycling in a global
5 three-dimensional model, *Global Biogeochemical Cycles*, 18, 10.1029/2004gb002220, 2004.
- 6 Moore, J. K., Doney, S. C., Lindsay, K., Mahowald, N., and Michaels, A. F.: Nitrogen fixation amplifies the
7 ocean biogeochemical response to decadal timescale variations in mineral dust deposition, *Tellus*
8 *Series B-Chemical and Physical Meteorology*, 58, 560-572, 10.1111/j.1600-0889.2006.00209.x, 2006.
- 9 Moore, J. K., and Doney, S. C.: Iron availability limits the ocean nitrogen inventory stabilizing feedbacks
10 between marine denitrification and nitrogen fixation, *Global Biogeochemical Cycles*, 21,
11 10.1029/2006gb002762, 2007.
- 12 Moore, J. K., Lindsay, K., Doney, S. C., Long, M. C., and Misumi, K.: Marine Ecosystem Dynamics and
13 Biogeochemical Cycling in the Community Earth System Model CESM1(BGC) : Comparison of the
14 1990s with the 2090s under the RCP4.5 and RCP8.5 Scenarios, *Journal of Climate*, 26, 9291-9312,
15 10.1175/jcli-d-12-00566.1, 2013.
- 16 Najjar, R. G., Sarmiento, J. L., and Toggweiler, J. R.: Downward transport and fate of organic matter
17 in the ocean: simulations with a general circulation model, *Global Biogeochemical Cycles*, 6,
18 45-76, 10.1029/91GB02718, 1992
- 19 Najjar, R. G., Jin, X., Louanchi, F., Aumont, O., Caldeira, K., Doney, S. C., Dutay, J. C., Follows, M., Gruber,
20 N., Joos, F., Lindsay, K., Maier-Reimer, E., Matear, R. J., Matsumoto, K., Monfray, P., Mouchet, A.,
21 Orr, J. C., Plattner, G. K., Sarmiento, J. L., Schlitzer, R., Slater, R. D., Weirig, M. F., Yamanaka, Y.,
22 and Yool, A.: Impact of circulation on export production, dissolved organic matter, and dissolved
23 oxygen in the ocean: Results from Phase II of the Ocean Carbon-cycle Model Intercomparison Project
24 (OCMIP-2), *Global Biogeochemical Cycles*, 21, 10.1029/2006gb002857, 2007.
- 25 Ono, T., Midorikawa, T., Watanabe, Y. W., Tadokoro, K., and Saino, T.: Temporal increases of phosphate and
26 apparent oxygen utilization in the subsurface waters of western subarctic Pacific from 1968 to 1998,
27 *Geophysical Research Letters*, 28, 3285-3288, 10.1029/2001gl012948, 2001.
- 28 Palmer, J. R., and Totterdell, I. J.: Production and export in a global ocean ecosystem model, *Deep-Sea*
29 *Research Part I-Oceanographic Research Papers*, 48, 1169-1198, 10.1016/s0967-0637(00)00080-7,
30 2001.
- 31 Paulmier, A., and Ruiz-Pino, D.: Oxygen minimum zones (OMZs) in the modern ocean, *Progress in*
32 *Oceanography*, 80, 113-128, 10.1016/j.pocean.2008.08.001, 2009.
- 33 Pierce, S. D., Barth, J. A., Shearman, R. K., and Erofeev, A. Y.: Declining Oxygen in the Northeast Pacific,

- 1 Journal of Physical Oceanography, 42, 495-501, 10.1175/jpo-d-11-0170.1, 2012.
- 2 Riahi, K., Rao, S., Krey, V., Cho, C., Chirkov, V., Fischer, G., Kindermann, G., Nakicenovic, N., and Rafaj,
3 P.: RCP 8.5-A scenario of comparatively high greenhouse gas emissions, Climatic Change, 109, 33-
4 57, 10.1007/s10584-011-0149-y, 2011.
- 5 Ridder, N. N., and England, M. H.: Sensitivity of ocean oxygenation to variations in tropical zonal wind stress
6 magnitude, Global Biogeochemical Cycles, 28, 909-926, 10.1002/2013gb004708, 2014.
- 7 Sallee, J. B., Shuckburgh, E., Bruneau, N., Meijers, A. J. S., Bracegirdle, T. J., and Wang, Z.: Assessment of
8 Southern Ocean mixed-layer depths in CMIP5 models: Historical bias and forcing response, Journal of
9 Geophysical Research-Oceans, 118, 1845-1862, 10.1002/jgrc.20157, 2013a.
- 10 Sallee, J. B., Shuckburgh, E., Bruneau, N., Meijers, A. J. S., Bracegirdle, T. J., Wang, Z., and Roy, T.:
11 Assessment of Southern Ocean water mass circulation and characteristics in CMIP5 models: Historical
12 bias and forcing response, Journal of Geophysical Research-Oceans, 118, 1830-1844,
13 10.1002/jgrc.20135, 2013b.
- 14 Seferian, R., Bopp, L., Gehlen, M., Orr, J. C., Ethe, C., Cadule, P., Aumont, O., Melia, D. S. Y., Voltaire, A.,
15 and Madec, G.: Skill assessment of three earth system models with common marine biogeochemistry,
16 Climate Dynamics, 40, 2549-2573, 10.1007/s00382-012-1362-8, 2013.
- 17 Seibel, B. A.: Critical oxygen levels and metabolic suppression in oceanic oxygen minimum zones,
18 The Journal of Experimental Biology, 214, 326-336, 10.1242/jeb.049171, 2011.
- 19 Sen Gupta, A., Santoso, A., Taschetto, A. S., Ummenhofer, C. C., Trevena, J., and England, M. H.: Projected
20 Changes to the Southern Hemisphere Ocean and Sea Ice in the IPCC AR4 Climate Models, Journal of
21 Climate, 22, 3047-3078, 10.1175/2008jcli2827.1, 2009.
- 22 Siegel, D. A., Buesseler, K. O., Doney, S. C., Salliey, S. F., Behrenfeld, M. J., and Boyd, P. W.: Global
23 assessment of ocean carbon export by combining satellite observations and food-web models, Global
24 Biogeochemical Cycles, 28, 181-196, 10.1002/2013gb004743, 2014.
- 25 Stramma, L., Johnson, G. C., Sprintall, J., and Mohrholz, V.: Expanding oxygen-minimum zones in the
26 tropical oceans, Science, 320, 655-658, 10.1126/science.1153847, 2008.
- 27 Stramma, L., Johnson, G. C., Firing, E., and Schmidtko, S.: Eastern Pacific oxygen minimum zones: Supply
28 paths and multidecadal changes, Journal of Geophysical Research-Oceans, 115,
29 10.1029/2009jc005976, 2010a.
- 30 Stramma, L., Schmidtko, S., Levin, L. A., and Johnson, G. C.: Ocean oxygen minima expansions and their
31 biological impacts, Deep-Sea Research Part I-Oceanographic Research Papers, 57, 587-595,
32 10.1016/j.dsr.2010.01.005, 2010b.

- 1 Stramma, L., Oschlies, A., and Schmidtko, S.: Mismatch between observed and modeled trends in dissolved
2 upper-ocean oxygen over the last 50 yr, *Biogeosciences*, 9, 4045-4057, 10.5194/bg-9-4045-2012,
3 2012.
- 4 Taylor, K. E., Stouffer, R. J., and Meehl, G. A.: AN OVERVIEW OF CMIP5 AND THE EXPERIMENT
5 DESIGN, *Bulletin of the American Meteorological Society*, 93, 485-498, 10.1175/bams-d-11-00094.1,
6 2012.
- 7 Tjiputra, J. F., Roelandt, C., Bentsen, M., Lawrence, D. M., Lorentzen, T., Schwinger, J., Seland, O., and
8 Heinze, C.: Evaluation of the carbon cycle components in the Norwegian Earth System Model
9 (NorESM), *Geoscientific Model Development*, 6, 301-325, 10.5194/gmd-6-301-2013, 2013.
- 10 Tsuchiya, M.: THE ORIGIN OF THE PACIFIC EQUATORIAL 13-DEGREES-C WATER, *Journal of*
11 *Physical Oceanography*, 11, 794-812, 10.1175/1520-0485(1981)011<0794:tootpe>2.0.co;2, 1981.
- 12 Vecchi, G. A., Soden, B. J., Wittenberg, A. T., Held, I. M., Leetmaa, A., and Harrison, M. J.: Weakening of
13 tropical Pacific atmospheric circulation due to anthropogenic forcing, *Nature*, 441, 73-76,
14 10.1038/nature04744, 2006.
- 15 Weijer, W., Sloyan, B. M., Maltrud, M. E., Jeffery, N., Hecht, M. W., Hartin, C. A., van Sebille, E., Wainer, I.,
16 and Landrum, L.: The Southern Ocean and Its Climate in CCSM4, *Journal of Climate*, 25, 2652-2675,
17 10.1175/jcli-d-11-00302.1, 2012.
- 18 Whitney, F. A., Freeland, H. J., and Robert, M.: Persistently declining oxygen levels in the interior waters of
19 the eastern subarctic Pacific, *Progress in Oceanography*, 75, 179-199, 10.1016/j.pocean.2007.08.007,
20 2007.
- 21 Williams, J. H. T., Totterdell, I. J., Halloran, P. R., and Valdes, P. J.: Numerical simulations of oceanic oxygen
22 cycling in the FAMOUS Earth-System model: FAMOUS-ES, version 1.0, *Geoscientific Model*
23 *Development*, 7, 1419-1431, 10.5194/gmd-7-1419-2014, 2014.
- 24 Yukimoto, S., et al.: Meteorological Research Institute-Earth System Model Version 1 (MRI-ESM1) Model
25 Description, Technical Reports of the Meteorological Research Institute No. 64, 2011
26
27
28

1 **List of Tables**

2 **Table 1:** Long-term trends in global oxygen and contribution from O₂sat and AOU across
 3 CMIP5 models (columns). The first row shows global oxygen during the historical period
 4 1960-1999, the second row shows relative change over 100 years from 1960-1999 to 2060-
 5 2099 (in %), and the third and fourth rows show the percentage of oxygen decrease due to a
 6 decrease in O₂sat and an increase in AOU. The last column shows the multi-model average
 7 and st. dev. by weighting models as described in Table A1.

8

	CESM1 -BGC	GFDL- ESM2G	GFDL- ESM2M	HadGEM2- ES (CC)	IPSL- CM5A- MR (LR)	MPI-ESM- MR (LR)	MRI- ESM1	NorES M1- ME	Multi- model Average (st.dev)
O₂ (mmol)	190.9	188.3	171.8	178.1 (177.0)	137.0 (148.4)	174.5 (176.1)	209.8	236.3	186.6 (26.0)
ΔO₂ /O₂ (%)	-3.1	-2.7	-3.5	-3.9 (-3.7)	-3.6 (-4.0)	-2.5 (-2.8)	-1.3	-1.3	-2.8 (0.9)
ΔO₂sat/ΔO₂ (%)	41.3	44.4	40.0	34.2 (33.5)	46.0 (38.0)	52.6 (49.7)	54.5	88.2	49.4 (15.9)
-ΔAOU/ΔO₂ (%)	58.7	55.6	60.0	65.8 (66.5)	54.0 (62.0)	47.4 (50.3)	45.5	11.8	50.6 (15.9)

9

10

11

12

13

14

15

16

17

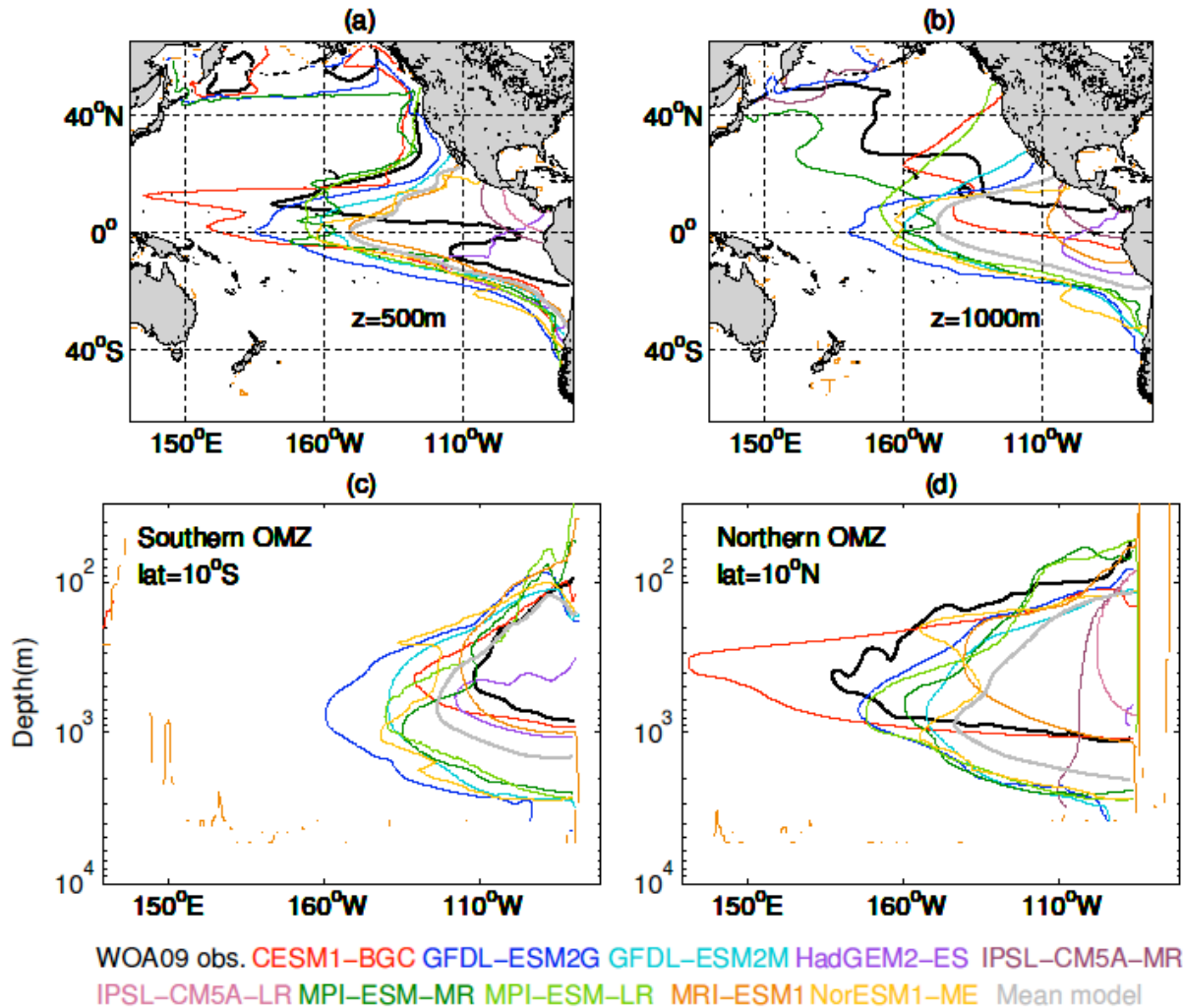
18

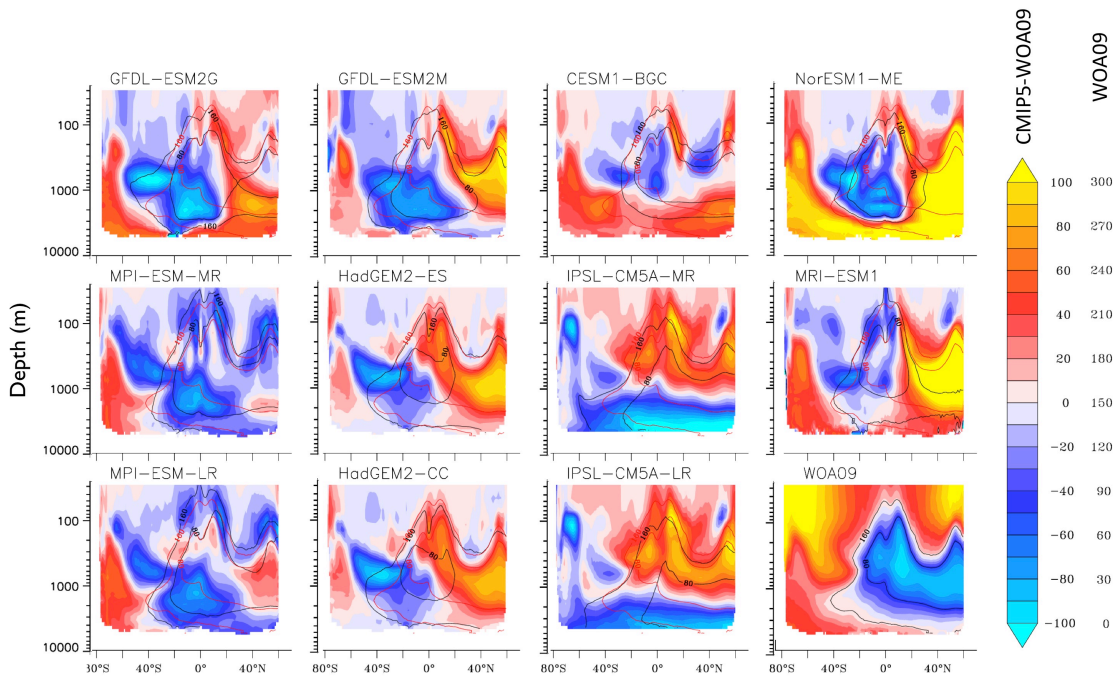
19

20

1 **List of Figures**

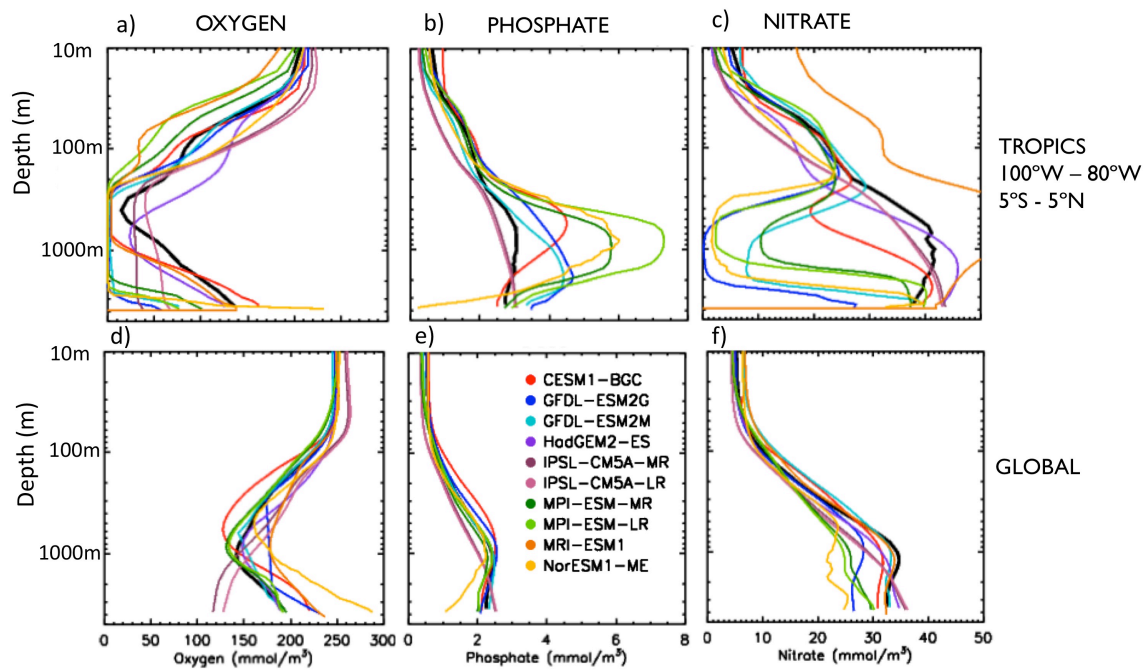
2





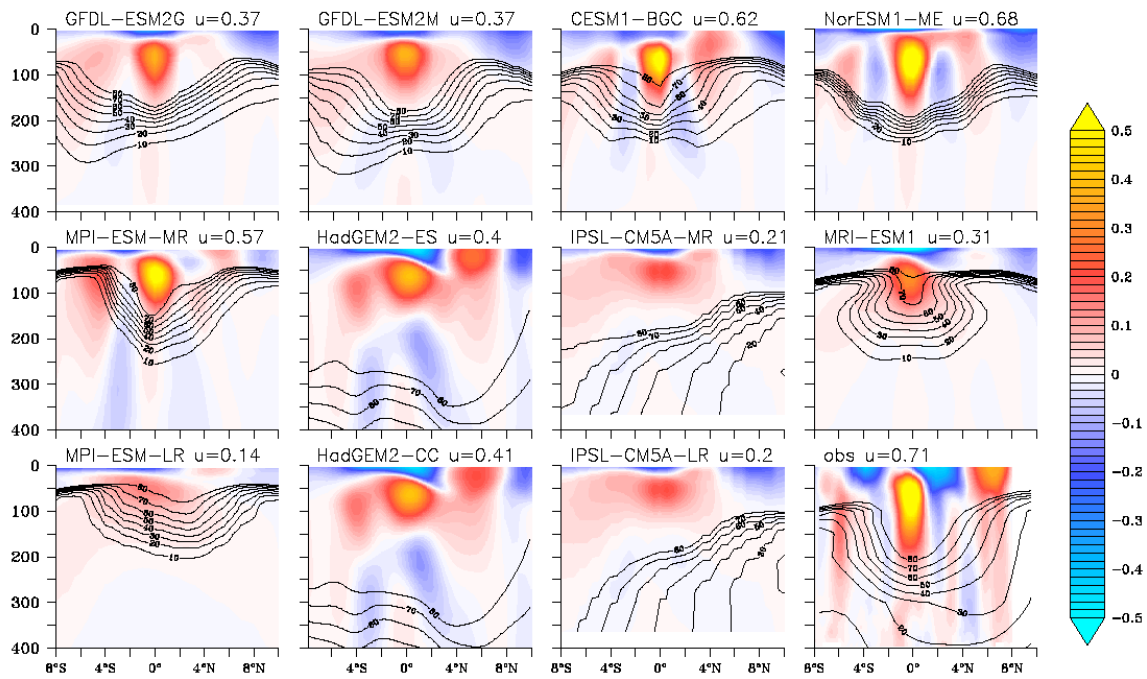
1
2
3
4
5
6
7
8
9
10
11
12
13
14
15

Figure 2. Differences between CMIP5 models' estimates and WOA09 climatological observations of oxygen concentration (mmol/m^3) zonally averaged from 160°W to 60°W in the Pacific at various depths and latitudes during the historical period (1960-1999). Last panel shows the corresponding zonal mean oxygen concentrations (mmol/m^3) from the observational WOA09 data set. In each panel, oxygen concentrations equal to 80 mmol/m^3 and 160 mmol/m^3 , respectively, are represented by superimposed contour lines (black for each model and red for observations).



1
 2 **Figure 3.** Average vertical profiles of (a) oxygen, (b) phosphate and (c) nitrate concentrations
 3 (mmol/m^3) from CMIP5 models (colored lines – explained in the legend) and the WOA09
 4 observations (black line) in the eastern tropical Pacific region spanning 80°W to 100°W
 5 longitude and 5°N to 5°S latitude. (d)-(f) Analogous global averages. **The model HadGEM2-**
 6 **CC (not shown) shows results similar to HadGEM2-ES.**

7
 8
 9
 10



1

2

3 **Figure 4.** Average equatorial ventilation (represented by the zonal component of velocity,
 4 m/s, shown in colors) and oxygen concentration (shown as black contour lines for 10, 30, 40,
 5 50, 60, 70, and 80 mmol/m³, respectively) in CMIP5 models and observations (last panel),
 6 with depth along a 95°W longitude section in the tropical west Pacific (10°N to 8°S latitude).
 7 Observed *u* velocity is from Johnson et al. (2002) while the oxygen observations are from
 8 WOA09. The dominant current shaping the OMZ in the east-west direction is the Equatorial
 9 Under Current, revealed by the high (red to yellow) velocities at the Equator. The maximum
 10 intensity of the EUC is labeled next to the model name (in m/s).

11

12

13

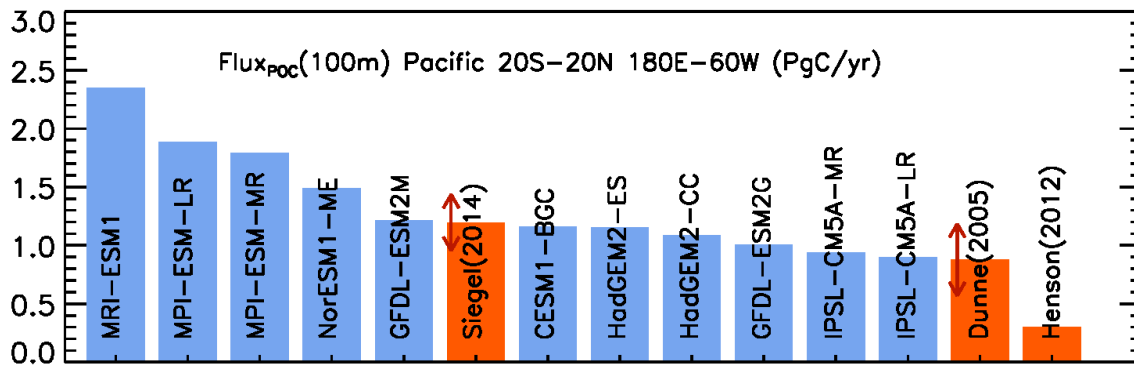
14

15

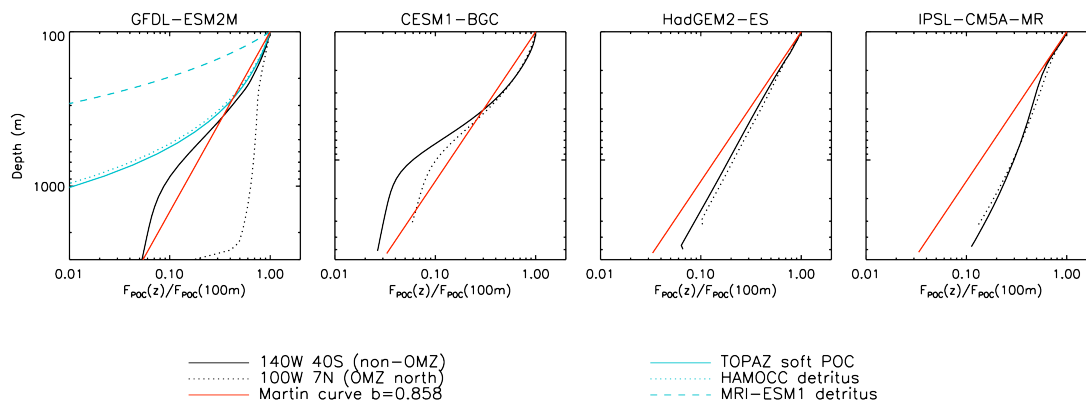
16

17

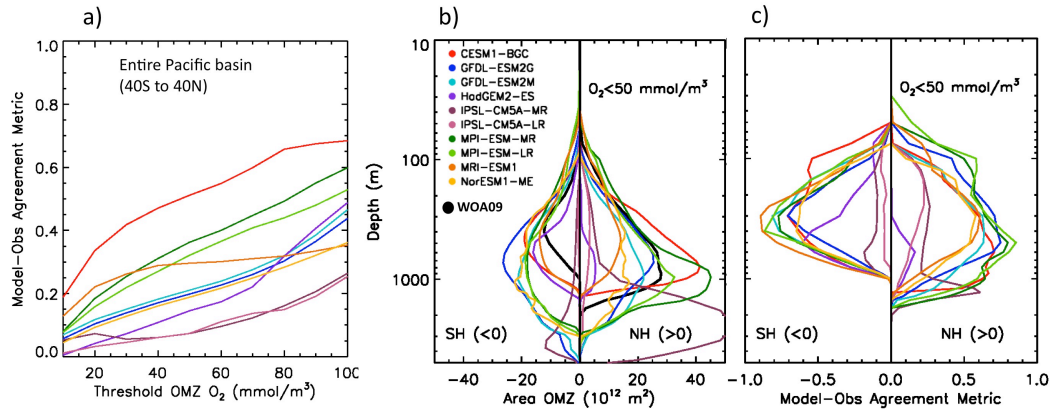
18



1
2 **Figure 5.** Total particulate organic carbon (POC) flux (Pg/year) at the depth of 100 m in the
3 eastern tropical Pacific (20°S to 20°N latitude and 180°E to 60°W longitude) estimated by each
4 of the CMIP5 models (blue) and derived from measurements (orange) by Dunne et al. (2005),
5 Henson et al. (2012), and Siegel et al. (2014). Results are ordered according to the flux
6 magnitude. Dunne et al. (2005) reported errors of 35% and Siegel et al. (2014) errors of 20%
7 (shown as arrows).

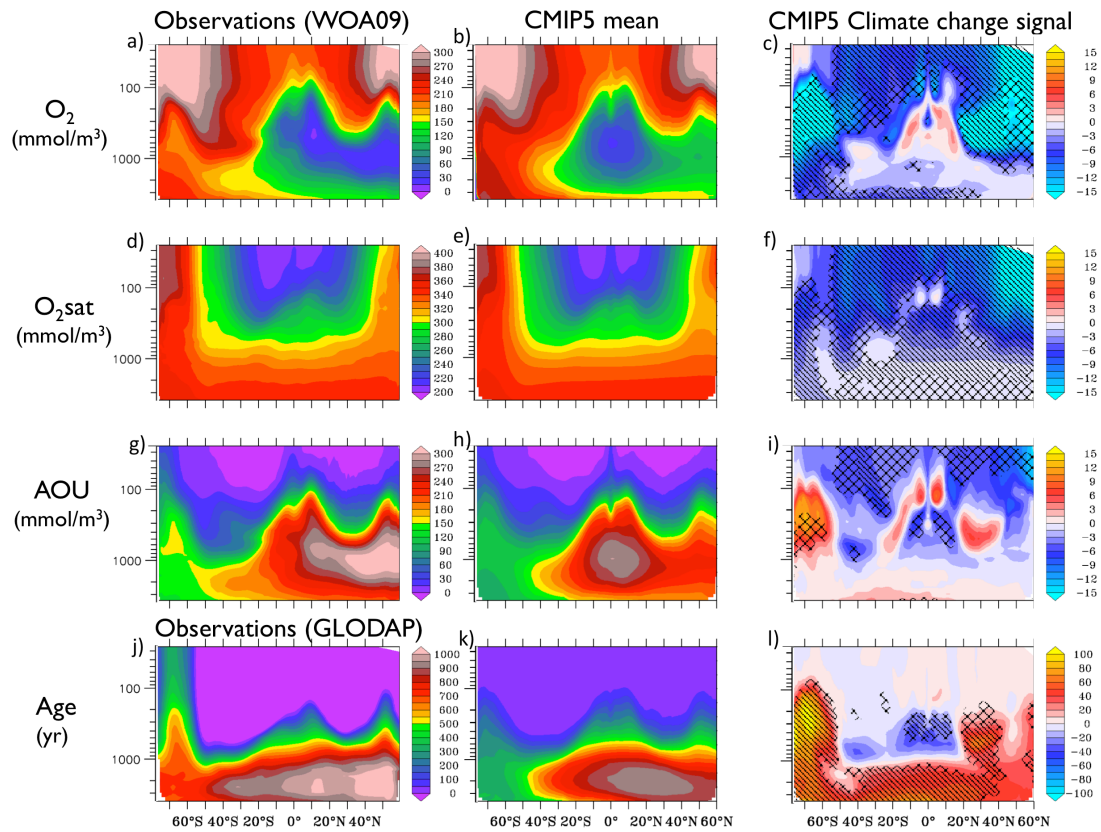


8
9 **Figure 6.** POC flux profile normalized to the value at 100m in the four CMIP5 models that
10 provided three-dimensional data: (a) GFDL-ESM2M, (b) CESM1-BGC, (c) HadGEM2-ES,
11 and (d) IPSL-CM5A-MR. The depth profile is shown for two locations, a typical non-OMZ
12 region at 40°S (solid black) and a typical OMZ (dashed black). The red line in each panel is a
13 power law with exponent 0.858 (Martin et al. 1987). Note that GFDL-ESM2M and CESM1-
14 BGC POC flux profiles are modeled as exponential curves, while IPSL-CM5A-MR and
15 HadGEM2-ES profiles are modeled as power laws (see equations in Table A3). In panel (a),
16 we also show the transfer efficiency for the exponential soft POC remineralization flux in
17 TOPAZ2 (GFDL-ESM2 models), HAMOCC (NorESM1-ME and MPI-ESM models), and
18 MRI-ESM1, all of them modeled as exponentials.



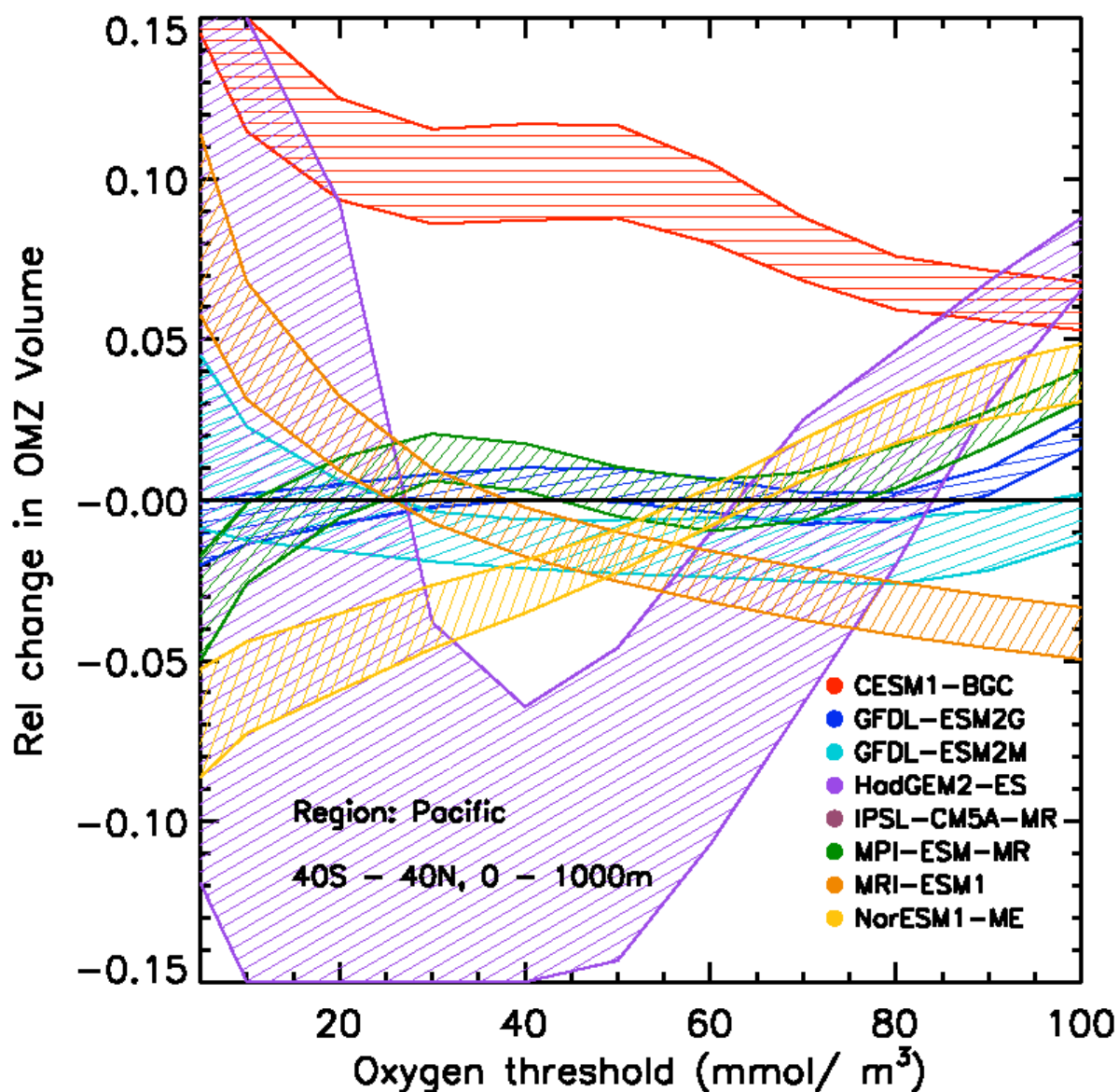
1
2 **Figure 7.** Agreement between modeled and observed OMZ extension in the Pacific during the
3 historical period (1960-1999). (a) The agreement of modeled OMZs with observations is
4 shown as the ocean volume that results from the intersection of the modeled and observed
5 OMZs, divided by the volume that encompasses both modeled and observed OMZs. The
6 OMZ volume is calculated at different O_2 thresholds (x axis). (b) Area of low-oxygen waters
7 ($O_2 < 50$ mmol/m³) at each depth across CMIP5 models and observations in the Southern
8 Hemisphere (0° - 40° S) (negative values) and in the Northern Hemisphere (0° - 40° N) (>0) as
9 labeled. (c) Agreement of modeled OMZs with observations at each depth, shown separately
10 for SH (0° - 40° S) (<0) and NH (0° - 40° N) (>0). The agreement is calculated as in (a) and goes
11 from 0 (no agreement) to 1 (perfect agreement). **The model HadGEM2-CC (not shown) shows**
12 **results similar to HadGEM2-ES.**

13
14
15



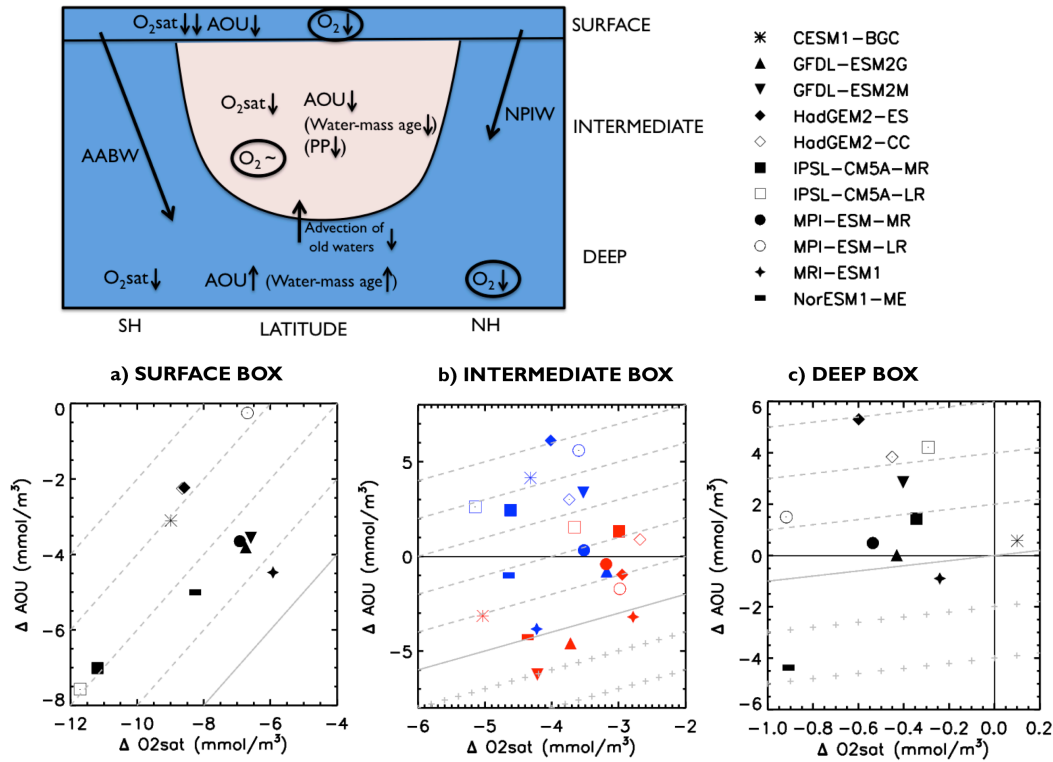
1
 2 **Figure 8.** Observational climatologies from WOA09 and GLODAP data sets (left column),
 3 CMIP5 multi-model mean historical simulations for the period 1960-1999 (middle column)
 4 and CMIP5 multi-model mean future projections for the period 2060-2099 referenced to the
 5 historical period (right column) for oxygen concentration (mmol/m^3) on the first row, O_2sat
 6 (mmol/m^3) on the second, AOU (mmol/m^3) on the third and water-mass age (yr) on the last
 7 row, all averaged zonally between 180°W and 100°W for a number of depths (y axis shows
 8 depth in m). The predicted 100-year change panels include diagonal pattern for trends that are
 9 consistent across CMIP5 models at the 90% level, and crossed patterns for 80% level. The
 10 observed age was multiplied by 2 in order to match qualitatively the CMIP5 magnitude. Only
 11 four of the studied models reported age. The metrics for 100-year change agreement is
 12 explained in the Methods section.

13
 14
 15

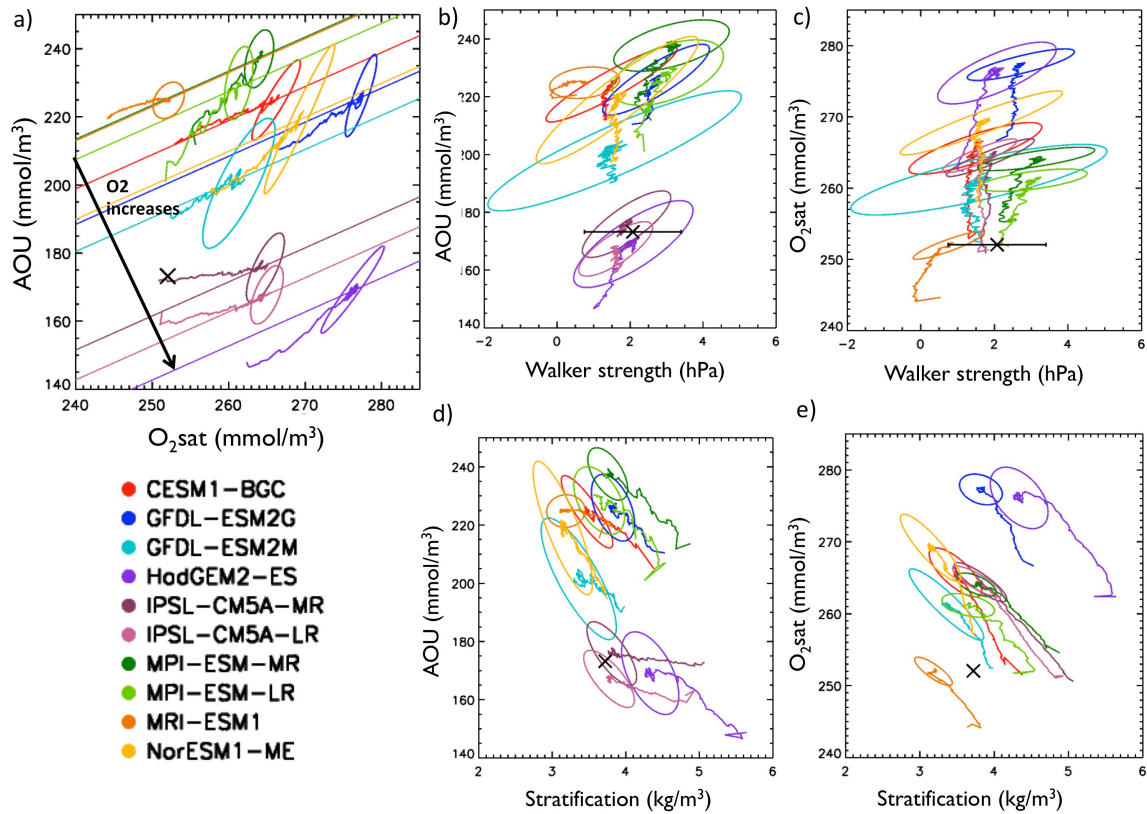


1
 2 **Figure 9.** Relative change in the volume of oxygen minimum zones in the Pacific between
 3 40°S and 40°N latitude to 1000m depth over 100 years (from the period 1960-1999 to the
 4 period 2060-2099) projected by individual CMIP5 models. Each model projection is shown as
 5 a patterned band that encompasses the natural variability (mean 100-year change \pm 1 standard
 6 deviation over 40 years in the control sample). MPI-ESM-LR and HadGEM2-CC are not
 7 shown for clarity, as these are very similar to MPI-ESM-MR and HadGEM2-ES. IPSL-
 8 CM5A-MR model lies outside of the plot limits and is shown in Sup. Fig. 7.

9
 10



1
 2 **Figure 10.** Top: Schematic of the 100-year change (1960-1999 to 2060-2099) in O₂ across
 3 CMIP5 models. Bottom: Relationship between the 100-year change in apparent oxygen
 4 utilization (ΔAOU , mmol/m³) and the analogous change in O₂sat ($\Delta O_2\text{sat}$, mmol/m³)
 5 estimated by individual CMIP5 models in the Pacific Ocean in (a) surface layer (average from
 6 50 m to 200 m), (b) intermediate layer (average from 200 to 1000 m) and (c) deep layer
 7 (average from 2000 to 4000 m). Solid gray lines in panels indicate no change in oxygen,
 8 dashed lines indicate decrease in oxygen concentration (-), and plus lines indicate increase in
 9 oxygen (+). In the intermediate box, low latitude values are represented in red (coinciding
 10 with decrease in multi-model mean age of at least 20 years) and high latitudes, i.e. zones of
 11 water formation (where age increases), are shown in blue.
 12



1
2
3
4
5
6
7
8
9
10
11
12
13
14
15
16

Figure 11. Interannual variability and climate-change trend in oxygen, AOU, and O₂sat for each CMIP5 model (symbolized by colors explained in the legend) in the eastern Pacific (from 10°S to 10°N latitude and 115°W to 60°W longitude) at a depth of 100 to 200 m. Solid lines denote constant oxygen values ($O_2 = O_{2\text{sat}} - \text{AOU}$) at the pre-industrial concentration. Each ellipse encompasses 95% of the interannual variability in O₂sat (x axis) and AOU (y axis), calculated in a 100-year period of the control run (a). The wiggly line shows the 20-year smoothed climate change evolution from 1900 to 2099, starting from the center of the ellipse and moving out of it as time passes. Observations are shown as a cross (WOA09). Subsequent panels show the effect of the Walker circulation strength on AOU (b) and O₂sat (c), and the effect of stratification on AOU (d) and O₂sat (e). Observed variability in Walker circulation is included in panels b and c (black line). **The model HadGEM2-CC (not shown) shows results similar to HadGEM2-ES.**